Biogenic preparation of ZnO nanostructures using leafy spinach extract for high-performance photodegradation of methylene blue under the illumination of natural sunlight

Mansab Ali Jakhrani, Muhammad Ali Bhatti, Aneela Tahira, Aqeel Ahmed Shah, Elmuez A. Dawi, Brigitte Vigolo, Ayman Nafady, Lama M. Saleem, A. Haj Ismail, Zafar Hussain Ibupoto

Biogenic preparation of ZnO nanostructures using spinach leafy extract for high performance photodegradation of methylene blue under the illumination of natural sunlight

Mansab Ali Jakhrani[1], Muhammad Ali Bhatti[2], Aneela Tahira[4], Aqeel Ahmed Shah[9], Elmuez A. Dawi[5*], Brigitte Vigolo[6], Ayman Nafady[7], Lama M. Saleem[8], A. Haj Ismail[5], Zafar Hussain Ibupoto[3*]

[1]Institute of Physics, University of Sindh, Jamshoro, Pakistan.

[2]Institute of Environmental Sciences, University of Sindh Jamshoro, 76080, Sindh, Pakistan.

[3]Dr M.A Kazi Institute of Chemistry, University of Sindh Jamshoro, 76080, Sindh, Pakistan.

[4]Institute of Chemistry, Shah Abdul Latif University Khairpur Mirs, Sindh, Pakistan.

[5]Nonlinear Dynamics Research Centre (NDRC), Ajman University, P.O. Box 346, United Arab Emirates.

[6]Université de Lorraine, CNRS, IJL, F-54000 Nancy, France.

[7]Department of Chemistry, College of Science, King Saud University, Riyadh, Saudi Arabia.

[8]Biomolecular Science, Earth and life Science, Amsterdam University, De Boelelaan 1105/1081 HV Amsterdam, The Netherlands.

[9]Department of Metallurgy, NED university of Engineering and Technology, Karachi Pakistan

[*]Corresponding author (s):

Zafar Hussain Ibupoto (zaffar.ibhupoto@usindh.edu.pk)

Elmuez A. Dawi (e.dawi@ajman.ac.ae)

Abstract

To cope with environmental pollution caused by toxic emissions into water streams, high performance photocatalysts based on ZnO semiconductor materials are urgently needed. In this study, ZnO nanostructures are synthesized using spinach leafy extract using a biogenic approach. By using phytochemicals contained in spinach, ZnO nanorods are transformed into large clusters assembled with nanosheets with visible porous structures. Through X-ray diffraction, it has been demonstrated that spinach leafy extract prepared with ZnO is hexagonal in structure. Surface properties of ZnO were altered by using 10 mL, 20 mL, 30 mL and 40 mL quantities of spinach

leafy extract. The size of ZnO crystallites is typically 14 nanometers. In the presence of sunlight, ZnO nanostructures mineralized methylene blue. Studies investigated photocatalyst doses, dye concentrations, pH effects on dye solutions, and scavengers. The ZnO nanostructures prepared with 40 mL of spinach leafy extract outperformed the degradation efficiency of 99.9% for the MB, since hydroxyl radicals were primarily responsible for degradation. During degradation, first-order kinetics were observed. Spinach leafy extract could be used to develop novel photocatalysts for the production of solar hydrogen and environmental hydrogen.

Keywords: Spinach leafy extract, ZnO nanostructures, methylene blue, scavenger.

1. Introduction

In recent decades, the rapid growth of metropolitan cities has been known to be highly beneficial to the human society, but at the same time to be extremely detrimental to human health. Water resources are notoriously polluted due to the direct or indirect disposal of a wide range of hazardous waste materials, and this will pose a significant threat to having easy access to clean water in the coming decades [1-4]. The industrial sector produces hundreds of different products, including printing inks, pulp, paints, and plastics, all of which are produced using a large number of synthetic dyes. Some of these organic dyes are widely used in the textile industry and thrown into water streams without prior treatment [5-9]. In addition to organic dyes and insecticides, industrial waste water contains toxic compounds. Color is an intrinsic property of organic dyes that has a strong impact on water bodies as it limits the photons of light and lowers the amount of dissolved oxygen. In aquatic life, these toxic aspects of organic dyes cause chronic health issues and environmental problems. Taking out dye pollutants from industrial wastewater has been gaining intense attention worldwide as a means of maintaining a green environment and enhancing the existence of living organisms. Numerous techniques have been developed to accomplish this goal, such as adsorption, biodegradation, and heterogeneous photocatalysis [10,11]. Nanostructured materials have recently been found to be effective protocols to remove organic dyes from wastewater due to their low dimensions and high surface-to-volume ratio. As well, specific affinity carrying agents further improve the surface effectiveness of removing dyes [12, 13]. Consequently, a series of functional nanostructured materials have been reported as photocatalysts, including ZnO [14, 15], Fe_2O_3 [16], TiO_2 [17], and WO_3 [18]. A number of

strategies are being developed to overcome the challenges associated with wastewater treatment in order to photodegrade these dyes from aqueous solutions.

Among the various designs of photocatalysts, semiconducting photocatalysts have proven to be highly effective. Research on the proposed project aims at enhancing photocatalysis through the development of new classes of materials or the modification of surfaces. Therefore, a great deal of research has been conducted regarding the development of active photocatalytic materials [19-31]. In comparison to other metal oxide semiconductors, titanium dioxide (TiO_2) is effective in removing dyes from water effluents, but it has been well explored to synthesize inexpensive ZnO photocatalysts for removing synthetic organic dyes from aqueous solutions [32-34]. ZnO has wide bandgap (3.37eV) and high electron mobility (60 meV) owing to its high electron-hole binding energy [35]. Among its many properties, ZnO is also well-known for its thermal, mechanical, piezoelectric, as well as optoelectronic properties. It has been reported that ZnO nanostructures have demonstrated outstanding photocatalytic and quantum properties over TiO_2 nanostructures which are commonly used in photocatalysis [36-39]. While physicochemical techniques are widely used for the synthesis of ZnO, these methods are limited by the use of costly and hazardous chemicals. Meanwhile, the green preparation of ZnO nanostructures is gaining a lot of popularity among researchers as it is ecofriendly, simple, environmentally friendly, and can be scaled up, making it an effective method for removing organic dyes from industrial wastewater effluents. In green preparation methods, there is no use of organic solvents, surfactants, or other chemicals. It has been demonstrated that the green synthesis of ZnO nanostructures using plant extracts allows for the retention of the crystal phase and allows for high surface modification in order to achieve efficient photocatalytic applications [40, 41]. Due to this, green preparation methods can serve as a promising alternative to physicochemical methods. A large number of phytochemicals can be found in plant extracts, which are capable of acting as reducing and/or stabilizing agents during the synthesis of nanostructured materials [42]. Alkaloids, phenols, glycosides, passifloricins, flavonoids, cyanogenic substances, polypeptides, and alpha pyrones are some of the phytochemicals that have been useful for preparing nanostructured materials [43-45]. *Spinach (Spinacia oleracea)* is an edible green vegetable that consists primarily of leaves. It belongs to the *Amaranthaceae family*. The growth of spinach generally takes place once a year and is a highly valued food constituent that contains antioxidants and anti-cancer properties. Spinach primarily contains vitamins A, C, K, and folate

as well as fiber, calcium, iron, and potassium [46]. Researchers have used spinach to grow ZnO nanostructures and study their applications [47-49].

Moreover, the spinach was used to its abundant crop production around the world, and we used the green leaves of spinach and collect the extract. There is no report about the transformation of one dimensional (ID) nanorod of ZnO into cluster formation using leafy extract of spinach due to the presence of various phytochemicals. These phytochemicals have properties of stabilizing agent, capping agent, chelating agent, and reducing agent which together play a vital role in tuning the surface properties of ZnO. These features of leafy extract of spinach have never been highlighted and investigated for the photocatalytic applications. As a consequence of these previous studies involving the preparation of ZnO from spinach leaf extract, it is evident that the spinach derived ZnO nanostructures have not been investigated for the Photodegradation of methylene blue (MB) under the irradiation of natural sunlight. Hence, for the first time, we are highlighting the use of it in biogenic ZnO synthesis and its contribution to removing MB green to nearly 100% under natural sunlight.

In this study, we have used the leafy extract of spinach for the surface alteration of ZnO nanostructures during hydrothermal process. The ZnO nanostructures were investigated with respect to morphology and crystal quality. The spinach leafy extract added vital role towards the enhancement of photocatalytic activity of ZnO nanostructures against methylene blue (MB) in aqueous solution.

2. Material and method

2.1. Used chemical reagents

The chemicals and reagents used in this study were of analytical grade without further purification. Merck provided the metal precursor zinc acetate dihydrate ($ZnC_4H_6O_4$ of 99.9% purity), and (ammonium solution 25%) for the experiment. Methylene blue ($C_{16}H_{18}ClN_3S$), silver nitrate, ascorbic acid were purchased from Sigma Aldrich Karachi Pakistan.

2.2. Preparation of leafy extract of *Spinacia oleracea*

Spinacia oleracea was purchased from the local market in Jamshoro, Sindh. During the extraction process, *Spinacia oleracea (S. oleracea)* leaves were thoroughly cleaned with deionized (DI) water in order to remove any dirt. To produce the paste, the preprocessed leaves (4 g wt%) were shredded into small pieces and placed in the juicer machine along with an appropriate quantity of DI water. Once the paste had been formed, it was transferred for filtration, and the filtration was repeated in order to proceed with the synthesis.

2.3. Green synthesis of ZnO in the presence of leafy extract of *Spinacia oleracea*

Our typical synthesis process included mixing already filtered leafy extract of S. oleracea (10 mL, 20 mL, 30 mL, and 40 mL) with 2.22g of zinc acetate dihydrate into four beakers, followed by adding 5mL of 25% ammonium solution, the samples specification given in Table 1. Meanwhile, we prepared 2.22g of zinc acetate without the leaf extract and named it pure ZnO. As well, each of 5 total beakers was covered with aluminum foil and placed in a preheated electric oven at 95^0 C for 5 hours. Precipitations were allowed to settle at room temperature (RT) before being filtered. Developed material was washed with ethanol and DI water, dried at 120 °C for 4 hours, and then burnt at 300 °C for 2 hours before being converted into fine and homogeneous powder (ZnO NPs) with the help of a mortar and pestle. A brief representation of synthesis process of ZnO nanostructures with spinach leafy extract is shown in Scheme 1.

2.4. Characterization of ZnO nanostructures

The pure ZnO samples and green synthesized ZnO samples were characterized for crystal structure information by recording the X-ray diffraction patterns (XRD) on the diffractometer (D8, Advance, Bruker, Germany) using the CuKα (1.542Å) beam as the radiation source in the range of 20–80 (2θ diffraction angles). SEM morphology of all materials was examined with the Nova Nano SEM, which has a magnification range of 20-200,000x and a resolution of up to 1 nm. We measured the concentration of methylene blue dye during the photodegradation reaction using a UV-visible spectrophotometer (Lambda365, Perkin Elmer, Walthem, MA, USA) [1].

2.5. Photocatalytic application of surface modified ZnO nanostructures

In this study, pure ZnO and green synthesized ZnO samples were photodegraded against a cationic dye (MB) under sunlight irradiation. Before photodegradation experiment, the initial methylene blue (MB) dye concentrations (8.22×10^{-5} M) and (6.12×10^{-5} M) were prepared and different catalyst material of each (5 mg, 10 mg and 15 mg) separately were placed in the five beakers possessing 50 mL of (8.22×10^{-5} M) and (6.12×10^{-5} M) methylene blue dye at constant stirring under dark conditions for 60 min, resulting in the formation of adsorption-desorption equilibrium. It has been reported elsewhere an average MB dye in waste water could be found 2-2.28 mg/L. Further, the pH of the solution mixture of MB was adjusted by adding either 0.050 M of NaOH or 0.050 M of H_2SO_4. Then, the solution mixture with the photocatalyst was placed in an open atmosphere and the solution was illuminated with sunlight, which enabled the activation of green ZnO material. Following this, two milliliters of each MB dye solution were injected into a quartz cuvette cell of one centimeter diameter at predetermined intervals (30 minutes), and the reduction in absorbance values was measured using a UV-Vis spectrophotometer. In order to determine the dye removal percentage of pure ZnO and green synthesized ZnO samples against methylene blue dye, the following universal formula was adopted:

$$\text{Dye removal (\%)} = (C_0\text{-}C_t/C_0) \times 100.$$

Here, C_0 and C_t are referred as initial and final concentration of MB at reaction time (t) after adding the catalyst, respectively.

3. Results and discussion

3.1. Crystal arrays, morphological studies of surface modified ZnO nanostructures

Figure 1a shows the measured XRD diffraction patterns of ZnO nanostructures prepared from spinach leaf extracts. Various ZnO samples were analyzed by powder XRD, and several crystal lattice planes were observed (100), (101), (102), (110), (103) and (112) which were well-confirmed by the standard (JCPDS card no: 79-2205). In Figure 1b, XRD suggests the presence of the hexagonal phase of ZnO that has a typical Wurtzite structure. However, phytochemicals present in spinach leaf extract have shifted their two theta angles towards a higher angle. It is

evident from the crystallographic features of pristine ZnO and spinach leaf extract assisted ZnO samples that their crystal systems are identical. With the use of significant volumes of spinach leaf extract, a significant shift has been found due to the presence of high levels of phytochemicals, so a dominant two-theta angle has been observed. The shift in two-theta angle is higher for the sample-4 compare to other samples owing to high density of heavy biochemical molecules from leafy extract which might offer the stress during the crystal growth, consequently an obvious shift in two-theta angle was noticed for the sample-4. In an intriguing development, the shift in two-theta angles may contribute to the addition of defects to the crystal arrays of ZnO, which may enhance the photocatalytic performance of these nanostructures. Based on the results of the XRD study, ZnO has been successfully synthesized using spinach leaf extract. The Scherrer equation has also been used to calculate the average crystallite size based on XRD data [50, 51]. On average, crystallites are approximately 14 nm in size for sample 4 as given in Table 2. Figure 2 illustrates the measured SEM images of pristine ZnO nanostructures and spinach leaf extract-induced ZnO nanostructures for evaluating their morphology. Figure 2a illustrates the distinctive nanorod-like morphology of pristine ZnO, with a length of several microns and a diameter of 200-400 nm. In contrast, the morphology of ZnO was completely altered, resulting in thin nanosheets arranged into large clusters with a dimension of a few microns; Figure 2b-e. There is a strong indication that as spinach leaf extract volume increases, cluster size increases; however, in the large clusters, nanosheets appear to be arranged into clusters, indicating that phytochemicals play an influential role in tuning and transforming nanorod morphology into porous clusters of sheets. The shape transformation from nanorod to sheet oriented clusters through the presence of oxygenated terminal groups of phytochemical which possibly. Therefore, these porous sheets enclosed in large clusters are very effective at removing MB dye from aqueous solutions. This is demonstrated below in the section on photocatalytic applications. Several factors determine the type of morphology transformation, including the effectiveness of the reactants, the polarized environment, hydrophobic magnetism, the synthesis mechanism, and Vander Waal forces followed by electric fields. Moreover, the energy and kinetic aspects of the preparation also affect the morphology of the nanostructured material to be grown [52, 53]. After the reusability measurement for three cycles, the material stability in terms of morphology changes was studied by SEM analysis as shown in Figure 2f. It is obvious that the material retained its shape and structure, verifying its stability for long term reuse. Furthermore, the

optical bandgap energies of pure ZnO and green synthesized ZnO samples were investigated as shown in Figure 3. Kubelka-Maunk plots have been used to calculate the band gap of both materials [54].

$(\alpha hv)^2 = K (hv - E_g)$

Herein, h- Planck constant, v frequency of illumination light, α – absorbance coefficient and E_g- band gap and K- proportionality constant. The calculated bad gap values changes with increasing the amount of spinach leafy extract. Pure ZnO has an optical bad gap value of 3.10 eV, which is well in agreement with that reported in the literature [55]. In contrast, sample-1, sample-2, sample-3 and sample-4 of the green synthesized ZnO samples have 2.90 eV, 2.82 eV, 2.71 eV and 2.58 eV, respectively. It appears that insertion of spinach leaf extract reduces the bandgap, which facilitates electron transportation and contributes to degradation by photocatalysis.

3.2. The Photodegradation of methylene blue under natural sunlight using spinach leafy extract assisted ZnO nanostructures

3.2.1 Effect of catalyst dose and initial MB dye concentration

Our first step in studying the degradation of MB in aqueous solution has been to investigate the degradation of MB without the use of catalysts and under pristine ZnO illumination under natural sunlight prior to analyzing surface modified ZnO nanostructures with spinach towards photodegradation of MB in aqueous solution. A solution of 8.22×10^{-5}M of methylene blue (MB) was prepared and exposed to natural daylight, and a decrease in absorbance through UV-visible spectrophotometer was observed at various intervals of time as illustrated in Figure 4a. MB was observed to degrade at a negligible rate without a photocatalyst. Figure 4b-d shows that both kinetics and degradation efficiency of 5.2% could not be demonstrated by the MB under natural illumination in the absence of catalytic material. Therefore, MB requires a photocatalyst with a high degradation rate and efficiency. Based on the catalytic activity of pristine ZnO toward MB degradation as shown in Figure 5a, we selected a catalyst dose of 15 mg. When using pristine ZnO in natural sunlight, degradation kinetics were relatively rapid. However, the degradation performance was poor because of the fast charge recombination rate of electron-hole pairs and the limited number of catalytic sites present in ZnO. Figure 5b-c illustrates the degradation kinetics governed by pseudo first order as the reaction rate was directly related to the

concentration of MB. As can be seen in Figure 5d, pristine degradation efficiency for MB is approximately 57%. It is evident from the degradation analysis shown in Figures 4 and 5 that either MB degradation in the absence of catalyst or with pristine ZnO under the illumination of natural sunlight was insufficiently efficient. In order to achieve high performance photodegradation of MB, a new generation of photocatalyst is urgently required. This paper introduces these challenges of mineralization of MB into harmless products. Because of its carcinogenic nature and toxic effects on the environment, we proposed the use of phytochemicals from spinach leafy extract as a method of enhancing ZnO's catalytic performance and evaluating its role towards MB dye. MB degradation was evaluated using four samples of ZnO containing different quantities of spinach extract, such as 10 mL, 20 mL, 30 mL, and 40 mL. Spinach leafy extracts have been shown to alter crystal defects and the morphology of ZnO both using XRD and SEM. As a result of using four different amounts of spinach leaf extract, we were able to confirm that ZnO-based photocatalysts with outstanding photocatalytic performance are optimized. Next, we evaluated the performance of the newly developed photocatalyst by evaluating the different catalyst dose of each sample of ZnO grown with four different volumes of spinach leafy extract, as well as the initial dye concentration and pH of dye solution.

Figure 6a-d shows the UV-visible absorbance spectra of 5 mg of catalyst dose of four samples of ZnO and it could be viewed that the MB degradation of 8.22×10^{-5}M became prominent with the sample of ZnO prepared with 40 mL of spinach leafy extract. There is a linear relationship between the decrease in absorbance and the different intervals of time, as well as the absorbance decrease of the ZnO sample prepared with a higher concentration of phytochemicals from 40 mL of spinach leafy extract. In the SEM analysis, it was noted that the use of a large volume of spinach produced large clusters of ZnO with assembled nanosheets showing obvious porous. Thus, they were more effective at removing MB dye than samples prepared with 10, 20 and 30 mL spinach leafy extracts. It is evident from UV-visible absorbance spectra of MB in water that it has two peaks corresponding to monomers and dimers carried by MB, one at 664 nm and the other at 625 nm [56]. As a result of the hypsochromic effect, the 664 nm peak has shown blue shift towards lower wavelengths under natural sunlight illumination [57, 58]. As a result of surface modification of ZnO with leafy extract of spinach, the absorbance of MB was significantly reduced after 210 minutes, and the intensity difference between 664 and 615 nm disappeared, suggesting that monomers degrade more rapidly than dimers [59]. Two peaks at

664 nm were also observed to be decreasing in intensity and shifting to the blue region, which was caused by the N-demethylated degradation as well as the degradation of phenothiazine [60]. In Figure 7a-c, the relative concentrations are represented by C_t and C_0, where Ct is the illuminate concentration of MB with different illumination times, and C_0 is the dye concentration of MB in aqueous solution at the outset. It has been shown that the photocatalytic performance of ZnO prepared with different volumes of spinach leafy extract is dominated by the irradiation time, and the rate constant is calculated using the following relation [61], which depicts the first order reaction $Ln(C_0/C_t) = Kt$.

Figure 7a,b illustrates the kinetic relationship between $ln(C_0/C_t)$ and irradiation time. In the kinetic analysis, photodegradation of MB with ZnO nanostructures showed the rate constants to be approximately $3.25x10^{-3}$ min^{-1}, $5.95x10^{-3}$ min^{-1}, $1.31x10^{-2}$ min^{-1}, and $1.42x10^{-2}$ min^{-1} for the ZnO samples prepared with 10, 20, 30 and 40 mL of spinach leaf extract. As shown in Table 3, the degradation efficiency of four samples of ZnO was also calculated and sample 4 showed the highest degradation efficiency of 90%. It appears that the phytochemicals of spinach leafy extract contributed to the strong surface modification and tuned the optical properties of materials, which resulted in enhanced photocatalytic activity. The degradation performance against MB in 8.22×10^{-5}M was also evaluated by monitoring the change in absorbance spectrum after exposure to natural sunlight for varying periods of time using four samples of ZnO prepared with 10, 20, 30 and 40 mL of spinach leafy extract at 10 mg and 15 mg, respectively. Figure 8 and 9 show the UV-visible absorbance spectra of MB at 8.22×10^{-5}M and it could be noted that the absorbance linearly decreased with the irradiation time and the increase in the catalyst doses of various ZnO samples. For sample 4 of ZnO prepared with 40 mL of spinach leafy extract, the decrease in absorbance was more pronounced in both cases of 10 mg and 15 mg catalyst doses compared to the three other samples of ZnO prepared with 10, 20 and 30 mL volumes of spinach leafy extract. Figure 10 illustrates the reaction kinetics of MB degradation. It was found that degradation rate increased linearly with time for both photocatalyst doses of 10 mg and 15 mg, but degradation rate of 15 mg catalyst dose was higher compared to 10 mg catalyst dose in 8.22×10^{-5}M of MB. The removal of MB from aqueous solution using catalyst doses of 10 mg and 15 mg yielded first order kinetics, and the rate constants for the removal were $5.86x10^{-3}$ min^{-1}, 8.72×10^{-3} min^{-1}, 1.47×10^{-2} min^{-1} and 1.77×10^{-2} min^{-1} as shown in Table 3. The degradation efficiency was also evaluated for the photocatalyst doses of 10 mg and 15 mg for the effective

removal of MB 8.22×10^{-5}M and it was found a 9.68×10^{-3} min^{-1}, 1.12×10^{-2} min^{-1}, 1.18×10^{-2} min^{-1}, and 2.26×10^{-2} min^{-1} suggesting that the 15 mg of photocatalyst has shown higher degradation efficiency of about 99% as shown in Figure 10.

We have previously examined the effects of elevated concentrations of MB dye ($8.1x10^{-5}$M) on the photocatalytic effectiveness of ZnO nanostructures prepared with spinach leaf extract (40 mL). Here, we examine the effects of low concentrations of MB dye ($6.21x10^{-5}$M) on that performance. With MB dye irradiated with natural sunlight, our study evaluated the photocatalytic performance of ZnO sample 4 with catalyst doses of 5, 10, and 15 mg. In Figure 11, we show the UV-visible absorbance spectra. For each catalyst dose, the absorbance of MB dye solution quickly decreased. However, the 15 mg catalyst dose had an excellent decrease in absorbance, indicating the superior performance activity of the catalyst in MB degradation under natural sunlight. A catalyst dose of 15 mg of sample ZnO offered large surface contact to MB molecules which involved both adsorption and oxidation simultaneously. Nevertheless, oxidation predominated due to the high density of catalytic sites provided by the newly modified ZnO nanostructures with spinach leaf extract. Similarly the degradation kinetics was also evaluated for the MB solution using different catalyst doses of 5mg, 10 mg, and 15 mg of sample-4 as shown in Figure12a-b. The degradation kinetics was followed by pseudo first order kinetics as shown in Figure 12a, whereas degradation is highly dependent on the MB concentration as shown in Figure 12b. And degradation efficiency was found higher for the catalyst dose of 15 mg of sample-4 as shown in Figure 12c. In vitro experiments have shown that higher dye concentrations require large amounts of hydroxyl radicals in order to degrade dye molecules. However, the hydroxyl reactive species generated on the surface of the catalyst remain the same regardless of the used photon intensity, catalytic dose, or illumination time [62]. Due to this, when dye is used at high concentrations, the hydroxyl radicals generated are not sufficient to degrade dye, reducing the efficiency of photodegradation.

3.2.2 Effect of pH of dye solution on the photocatalytic performance of as prepared ZnO nanostructures

The pH of dye solution plays a determining role in the photocatalytic properties of nanostructured materials. This is because it controls the reaction kinetics of dye degradation and the production of hydroxyl radicals, which are dependent on pH [63, 64]. In the case of sample 4,

the catalyst dose was 15 mg and the pH of the dye solution 6.21×10^{-5} M was adjusted between 3, 6, 9 and 12 using the range shown in Fig13a-d. Dye solution pH affects the amount of charge flowing on the catalyst surface and the affinity of dye molecules for the catalyst surface [65]. Based on published work, the pHpzc (point of zero charge) of pure ZnO was about 8.1, whereas the pHpzc (point of zero charge) of the ZnO-based photocatalyst prepared with spinach leafy extract was about 9.3 [66]. As it is known, the catalyst surface has a net zero charge at pHpzc. When the pH is less than pHpzc, the catalyst surface is positively charged, and when the pH is greater than pHpzc, the catalyst surface is negatively charged. The pHpzc values of pristine ZnO of 8.1 indicate that a pH lower than 8.3 would result in a surface that has a net positive charge. In contrast, a pH higher than 8.3 would result in a surface that has a net negative charge. Similarly, the ZnO sample prepared with 40 mL of spinach leaf extract has a pHpzc of 9.3 as well as a largely negative surface charge [67]. By increasing the pH of dye solution, the kinetics was highly fast and the removal efficiency percentage was increased as shown in Figure 14a-c. Figure 14 illustrates how the positively protonated surface of ZnO is limited in its effectiveness for the removal of dye at low acidic pH values. On the other hand, at pH 12 hydroxyl radicals were most dominant in removing dye. This resulted in a more negative surface and an increased affinity for oxidizing cationic MB molecules, resulting in an outperform degradation efficiency [68]. The corresponding rate constant values for pH 3, 6, 9 and 12 was found as 4.95×10^{-3} min^{-1}, 1.79×10^{-2} min^{-1}, 2.75×10^{-2} min^{-1} and 5.05×10^{-2} min^{-1} % respectively. The overall photocatalytic performance of as prepared ZnO nanostructures for fast and better visualization is summarized in Table 3. To determine the stability of the photocatalyst, we conducted a reusability test for three cycles using the green synthesized sample. As illustrated in Figure 15, the results of the reusability test are presented in barographs. According to the figure, green generated material performed exceptionally well against the degradation of cationic MB dye in all reusability tests. The results of research have shown that the as-prepared samples are excellent, reusable photocatalysts that can be used in contaminated water to break down hazardous organic dyes. In addition, SEM analysis was performed to determine the stability of ZnO material in terms of shape after dye degradation, as shown in Figure 2 (f). Based on these results, it appears that the photocatalyst was reasonably stable and could be used for several degradation cycles.

3.2.3. Scavenger study for the identification of type of radical species participating in photodegradation of MB in aqueous solution

Using ZnO nanostructures prepared with spinach leafy extract, a scavenger study was conducted to identify the radicals predominating in the oxidation of MB as shown in Figure 16. In addition, metal oxide nanostructures were tested as a means of inhibiting degradation of MB 8.22×10^{-5}M under natural sunlight by mixing it with silver nitrate, ascorbic acid, and ethylenediamine tetracetate (EDTA) at a concentration of 10 mM. A dye's degradation is either dominated by radicals like hydroxyl (.OH), superoxide ($.O_2$), or by a concentration of electron-hole pairs. Specifically, it is shown that ($.O_2$) and hydroxyl (.OH) radicals are involved, so we performed a scavenger study as per the published results [69], and the degradation of efficiency has been linked to the presence of these radicals [70, 71]. Silver nitrate showed a large inhibition of MB degradation in this study, and is known to limit hydroxyl radical production. Therefore, it was concluded that hydroxyl radical species were the main radical species accelerating the degradation of MB. The photocatalytic activity of as prepared ZnO sample with 40 mL of spinach leafy extract was compared with already existing photocatalysts as given in Table 4. It is obvious that the activity of presented ZnO sample is superior in terms of low cost fabrication, facile, high degradation efficiency, ecofriendly and environmental friendly approach material synthesis compare to previous studies on the same topic. Hence, the presented photocatalyst can be utilized as an effective protocol for the removal of MB from the industrial wastewater samples.

4. Conclusions

In summary, phytochemicals from spinach leaf extract were used to modify the surface and morphology of ZnO nanostructures using the hydrothermal method. It was found that ZnO morphology consisted of large clusters assembled within thin nanosheets with a porous structure. XRD studies have demonstrated that ZnO has a hexagonal phase with a Wurtzite structure. Methylene blue was turned into harmless products by the use of modified ZnO nanostructures under natural sunlight illumination. According to the XRD study, the average crystallite size was 14 nm. Several parameters were considered for evaluating the photocatalytic properties of ZnO, including catalyst dose, initial dye concentration, pH of dye solution, and scavenger studies. MB photodegradation was studied using first-order kinetics. The optimal ZnO-based photocatalyst was found with a degradation efficiency of approximately 100% when using 40 mL of spinach

leaf extract. In the practical applications of environmental and industrial wastewater treatment, spinach leaf extracts have shown to be a promising resource for preparing high performance photocatalytic materials.

Acknowledgments

The authors would like to acknowledge the Higher Education Commission of Pakistan for its partial support of the project (NRPU/8350). The authors extend their sincere appreciation to Researchers Supporting Project number (RSP2023R79), King Saud University, Riyadh, Saudi Arabia, for partial funding of this work. The authors acknowledge partial funding from Ajman University, Grant IDs 2022-IRG-HBS-5 and 2022-RTG-HBS-02. Additionally, Brigitte Vigolog would like to thank the Microscopy, Microprobes, and Metallography (3M) platform at the Institut Jean Lamour (IJL, Nancy, France) for its TEM and SEM facilities.

Conflict of Interest

Authors have no conflict of interest in the presented research work.

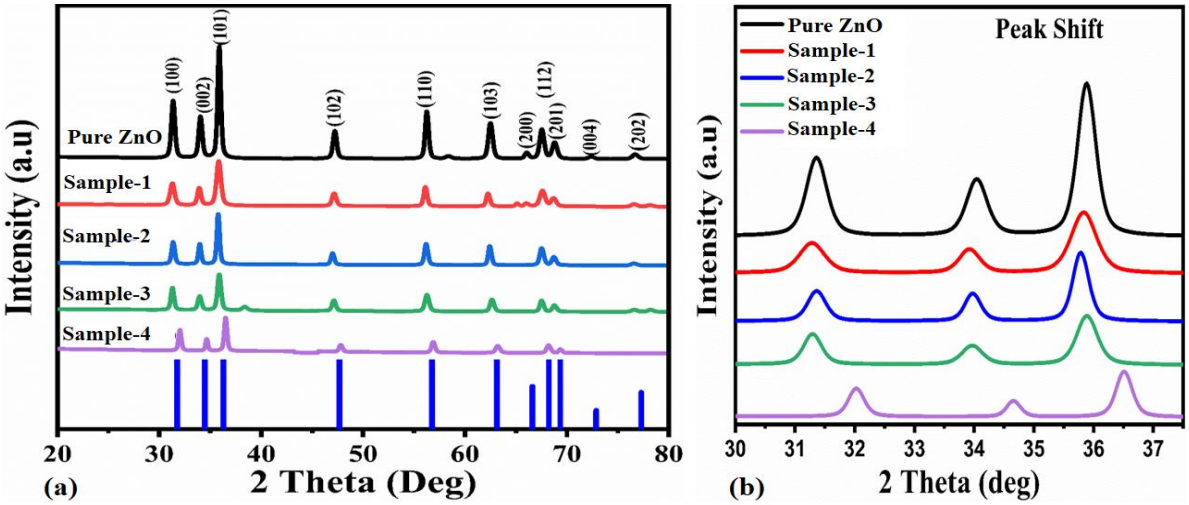

Figure1. (a) Powder XRD patterns of pure ZnO and green synthesized ZnO samples prepared with various amount of leafy extract of *S. oleracea* (10 mL, 20 mL, 30 mL and 40 mL) (b) illustrate the shift in (100), (002) and (101) Bragg reflections of as-synthesized samples.

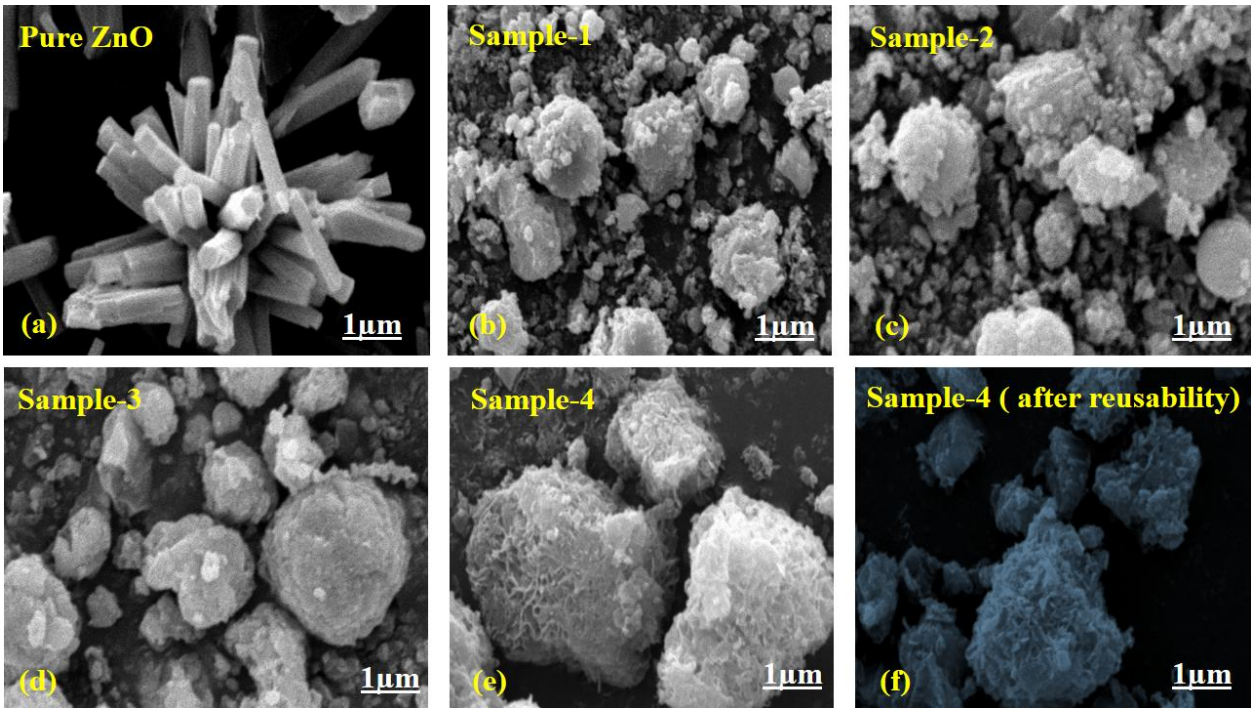

Figure 2. SEM images of (a) pure ZnO (b-e) green synthesized ZnO samples treated with different amounts of leafy extract of *S. oleracea* (10 mL, 20 mL, 30 mL and 40 mL) and (f) SEM image after reusability test.

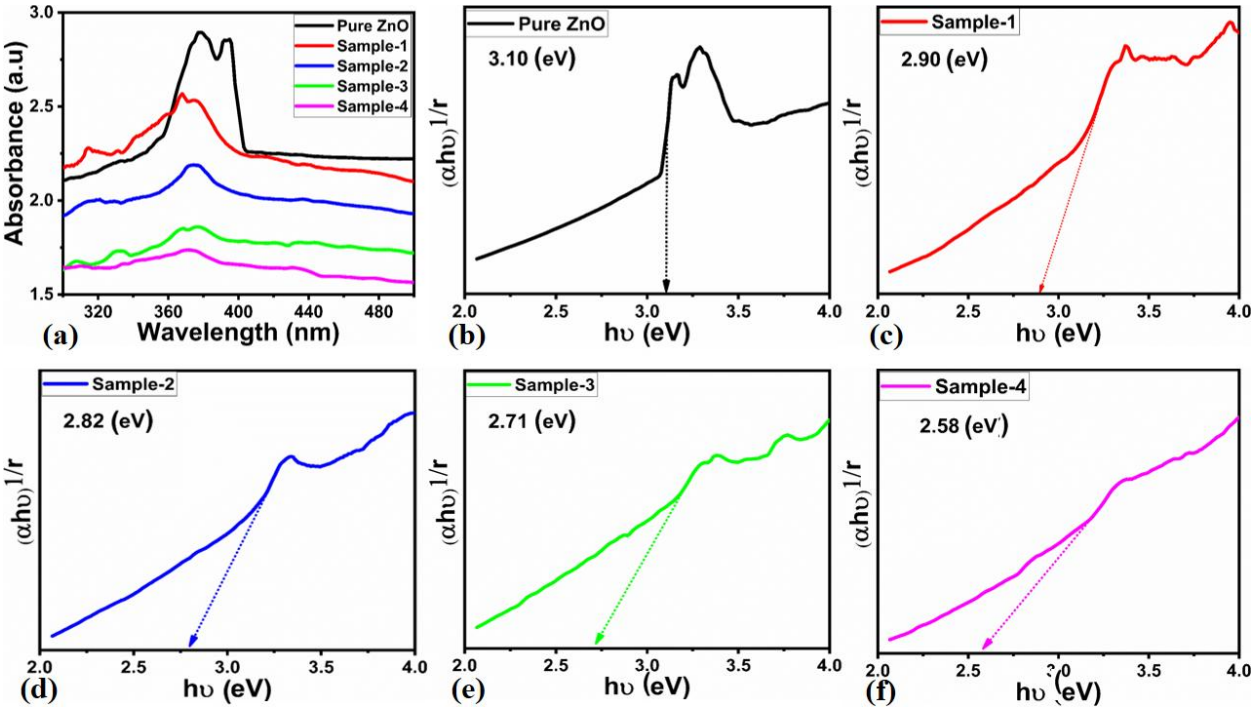

Figure 3: (a) UV- visible absorbance spectra of pure ZnO and sample-1, sample-2, sample-3, and sample-4, (b-f) Corresponding Kubelka–Munk plots

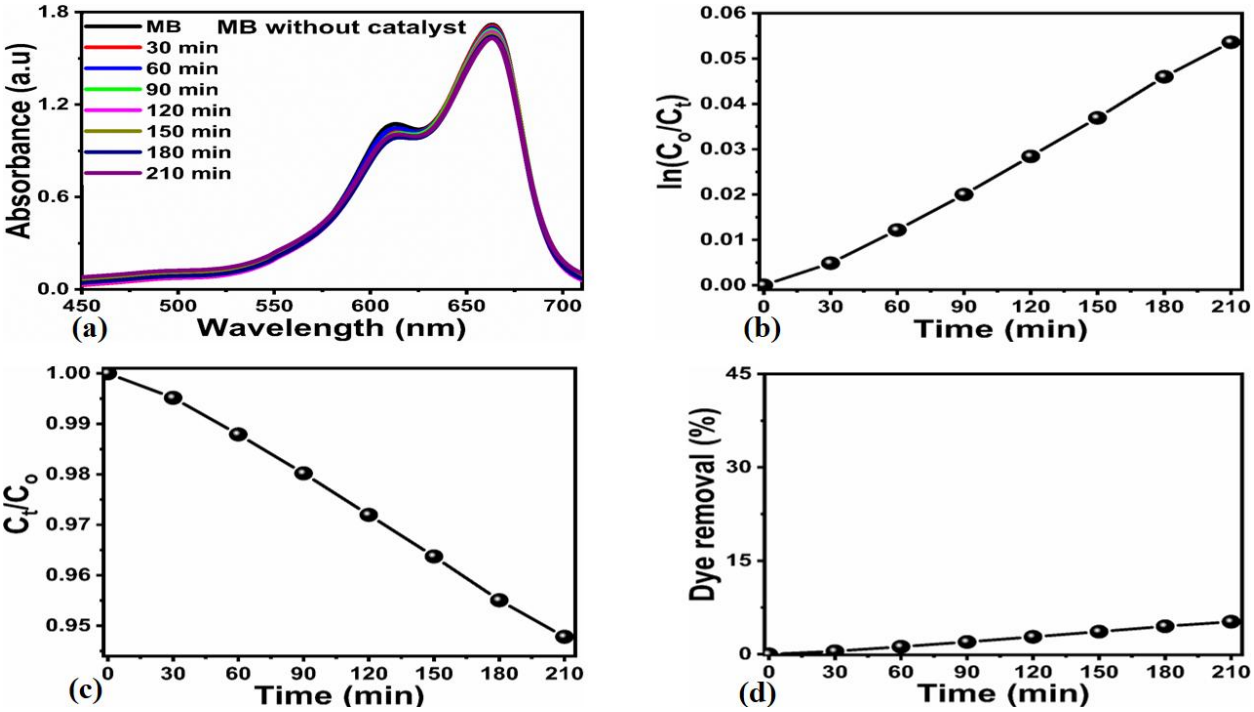

Figure 4. (**a**) UV-visible absorbance spectra measured in 8.22×10^{-5}M MB solution in the absence of catalyst with the irradiation of natural sunlight for the time interval of 210 min, (b) Linear plot of

Ln(C_t/C_o) against corresponding time of 210 min. (**c**) Linear plot of C_t/C_o. (**d**) Degradation efficiency of MB solution

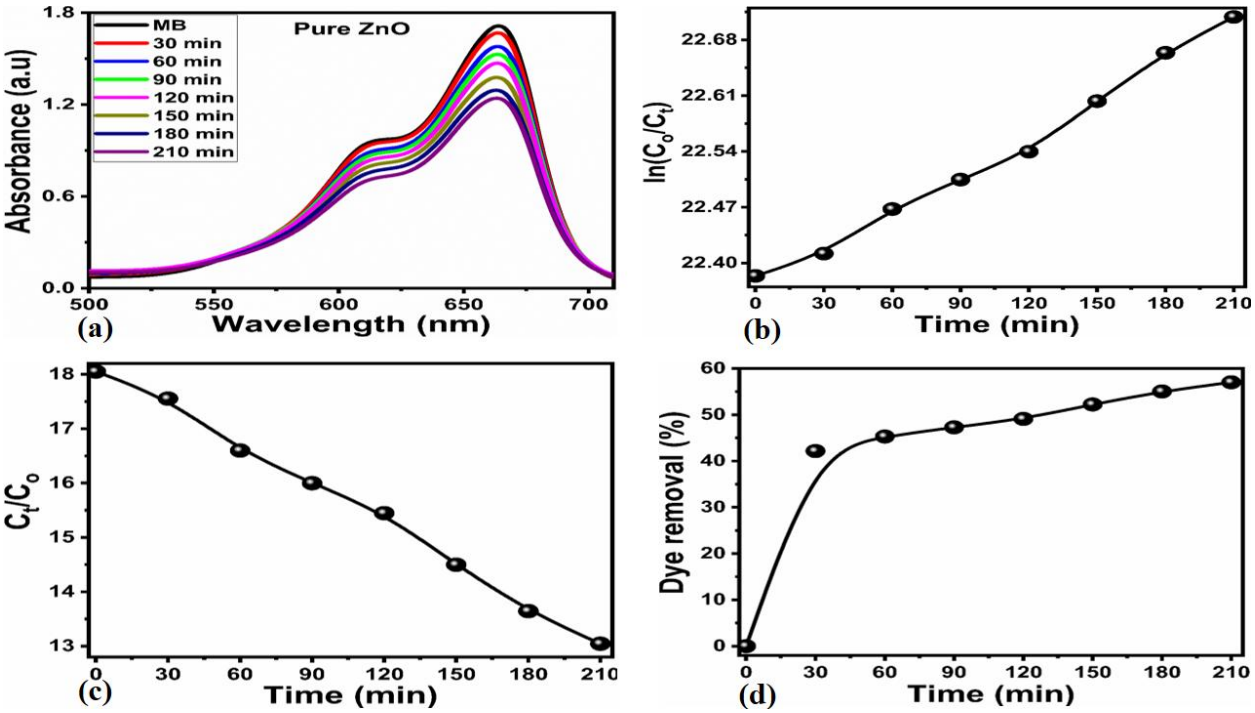

Figure 5. (a) UV-visible absorption spectra of 8.22×10^{-5} M) MB solution using photocatalyst dose of 15 mg of pure ZnO for the time interval of 210 min under the irradiation of natural sunlight,(b) Linear plot of Ln(C_t/C_o) against corresponding time of 210 min. (**c**) Linear plot of C_t/C_o. (**d**) Degradation efficiency of MB solution

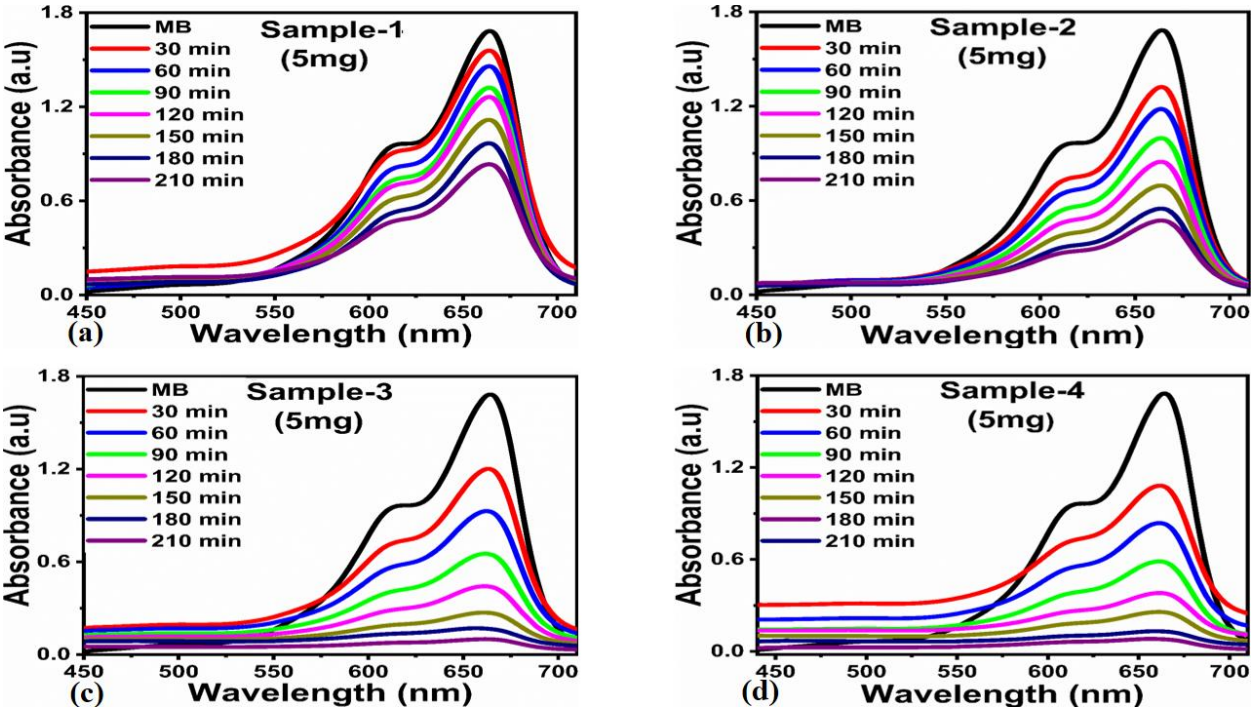

Figure 6. (a-d) UV-visible absorption spectra of photodegradation of 8.22×10^{-5}M) MB solution using catalyst dose of 5mg of sample-1, sample-2, sample-3 and sample-4 under the irradiation of natural sunlight

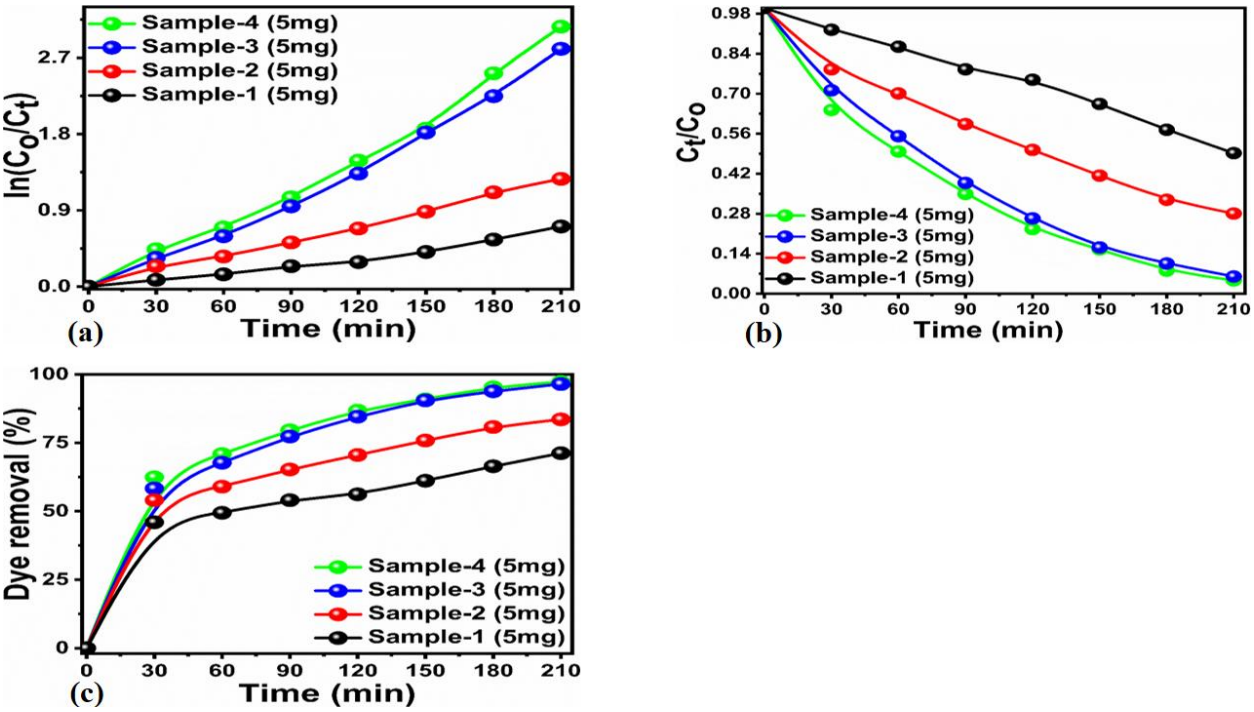

Figure 7. Photodegradation kinetics of 8.22×10^{-5}M) MB solution with catalyst dose of 5 mg of various samples of ZnO such as sample-1, sample-2, sample-3 and sample-4 under the irradiation of natural sunlight, (**a**) Linear plot of $Ln(C_t/C_o)$ against corresponding time of 210 min. (**b**) Linear plot of C_t/C_o. (**c**) Degradation efficiency of MB solution using catalyst dose of 5 mg of sample-1, sample-2, sample-3 and sample-4

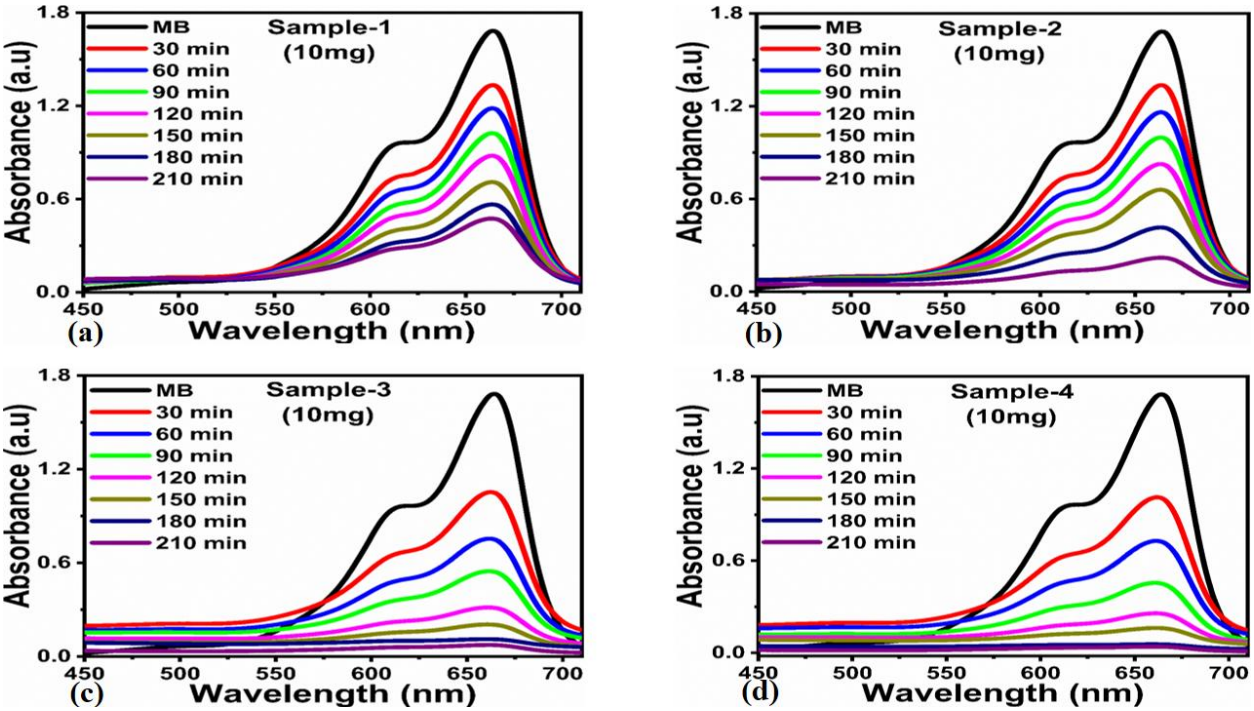

Figure 8. (a-d) UV-visible absorption spectra of photodegradation of 8.22×10^{-5}M) MB solution using catalyst dose of 10 mg of different ZnO samples including sample-1, sample-2, sample-3 and sample-4.

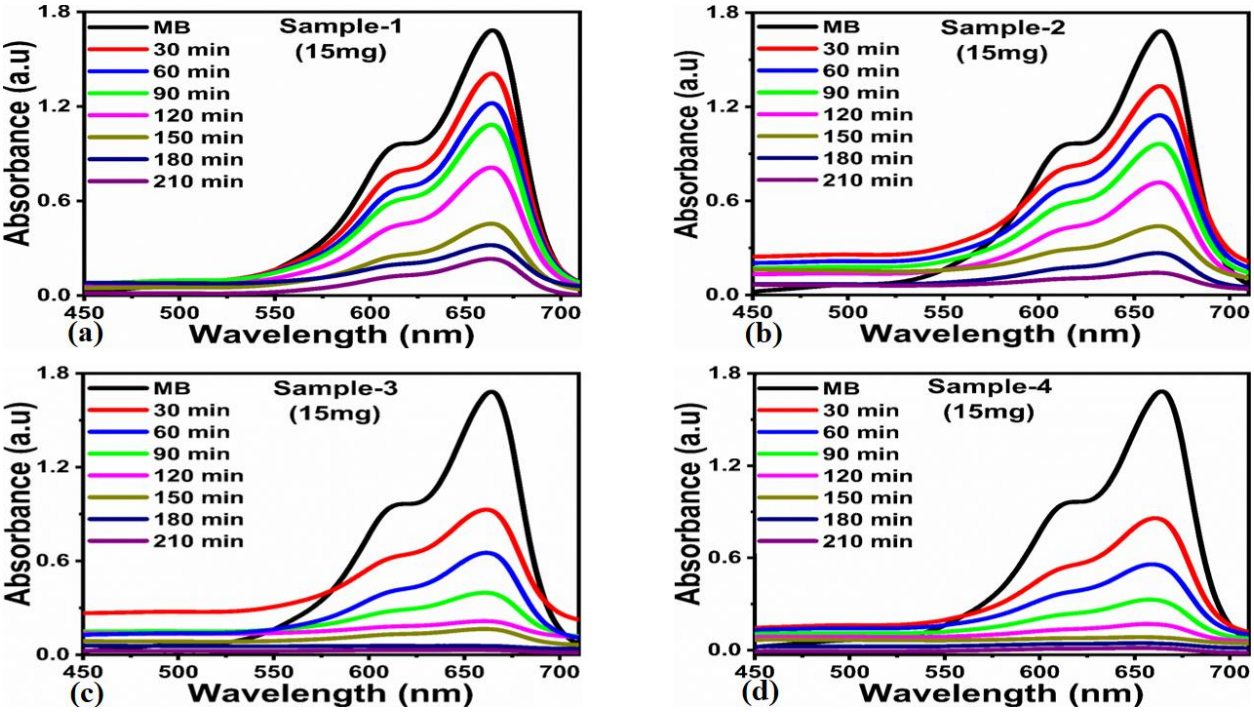

Figure 9. (a-d) UV-visible absorption spectra of photodegradation of 2.2×10^{-5}M) MB using catalyst dose of 15 mg of various ZnO samples such as sample-1, sample-2, sample-3, and sample-4

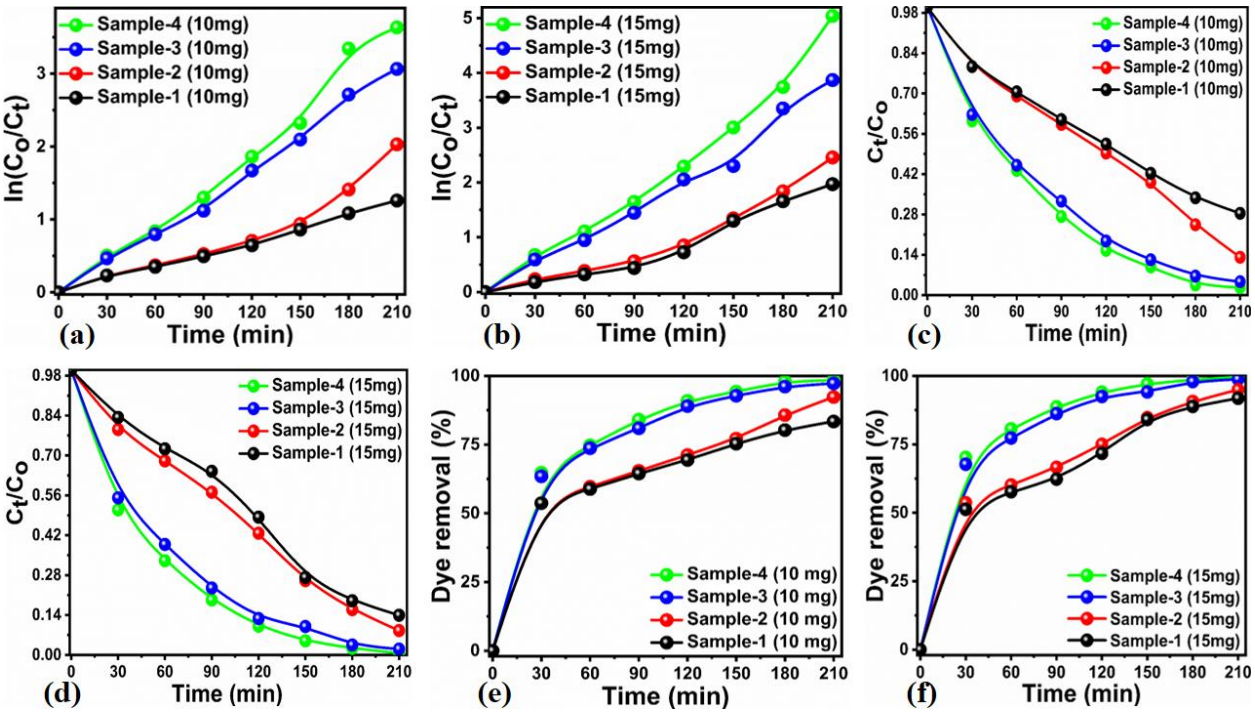

Figure 10. Degradation kinetics of MB using different catalyst doses of 10 and 15 mg in 8.22×10^{-5}M MB solution under the irradiation of natural sunlight. (**a**) Linear plot of $Ln(C_t/C_o)$ against 210 min for the catalyst dose of 10 mg, (**b**) Linear plot of $Ln(C_t/C_o)$ against 210 min for the catalyst dose of 15 mg , (c) Linear plot of C_t/C_o for the catalyst dose of 10 mg, (**d**) Linear plot of C_t/C_o for the catalyst dose of 15 mg, (e) Degradation efficiency of MB solution using catalyst dose of 10 mg, (**f**) Dye removal percentage dose of MB solution using 15 mg of catalyst dose

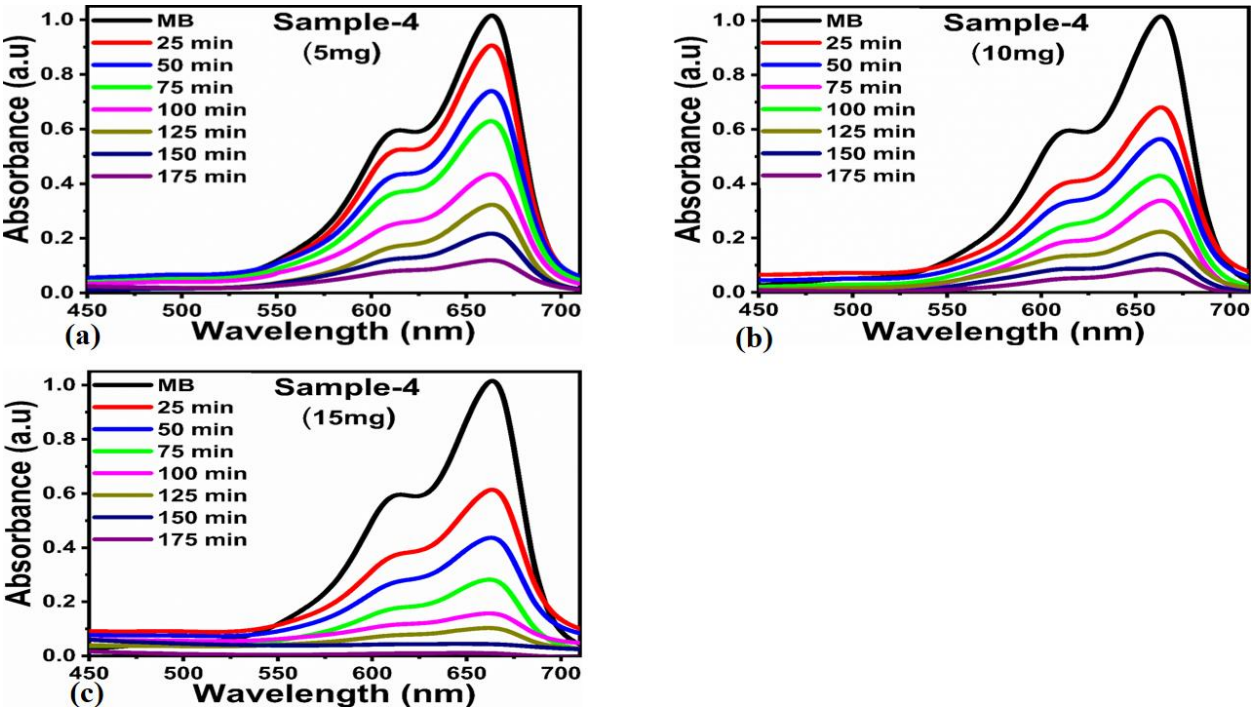

Figure 11. (a-c) UV-Visible absorption spectra of photodegradation of 6.12×10^{-5}M) MB solution using various catalyst doses uch as 5 mg, 10 mg and 15 mg of sample-4

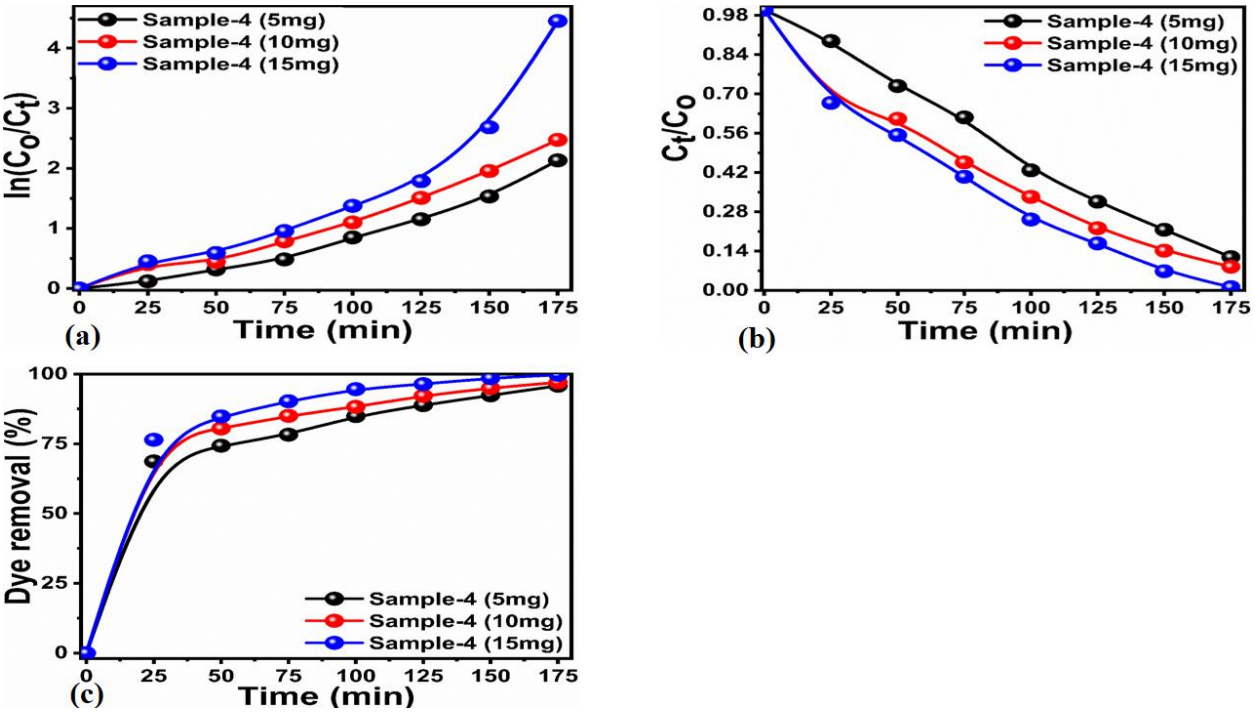

Figure 12. Photodegradation kinetics of 6.12×10^{-5}M) MB solution with various catalyst dose of 5 mg, 10 mg and 15 mg of sample-4 under irradiation of natural sunlight (**a**) Linear plot of $Ln(C_t/C_o)$ against corresponding time of 175 min. (**b**) Linear plot of C_t/C_o. (**c**) Various pH dependent degradation efficiency of MB solution.

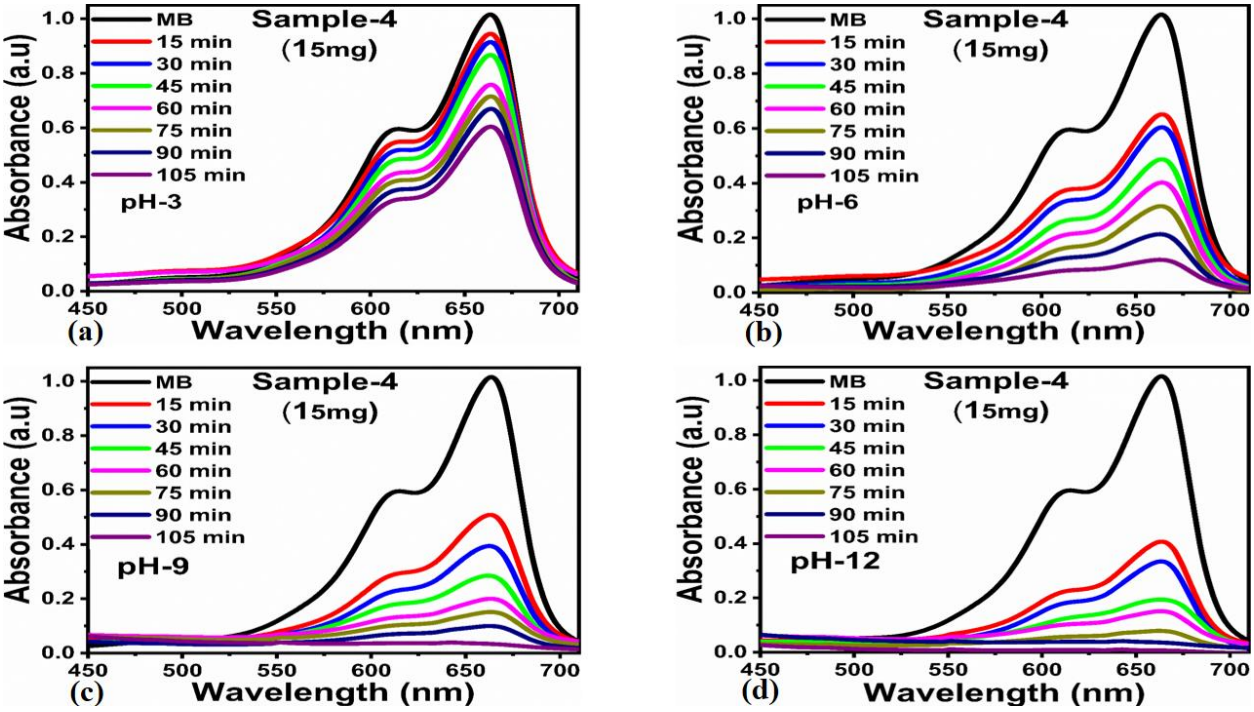

Figure 13. (**a**–**d**) UV- visible absorbance spectra measured for adjusted pH 3, 6, 9 and 12 of 6.12×10^{-5} M MB solution using catalyst dose of15 mg of sample-4.

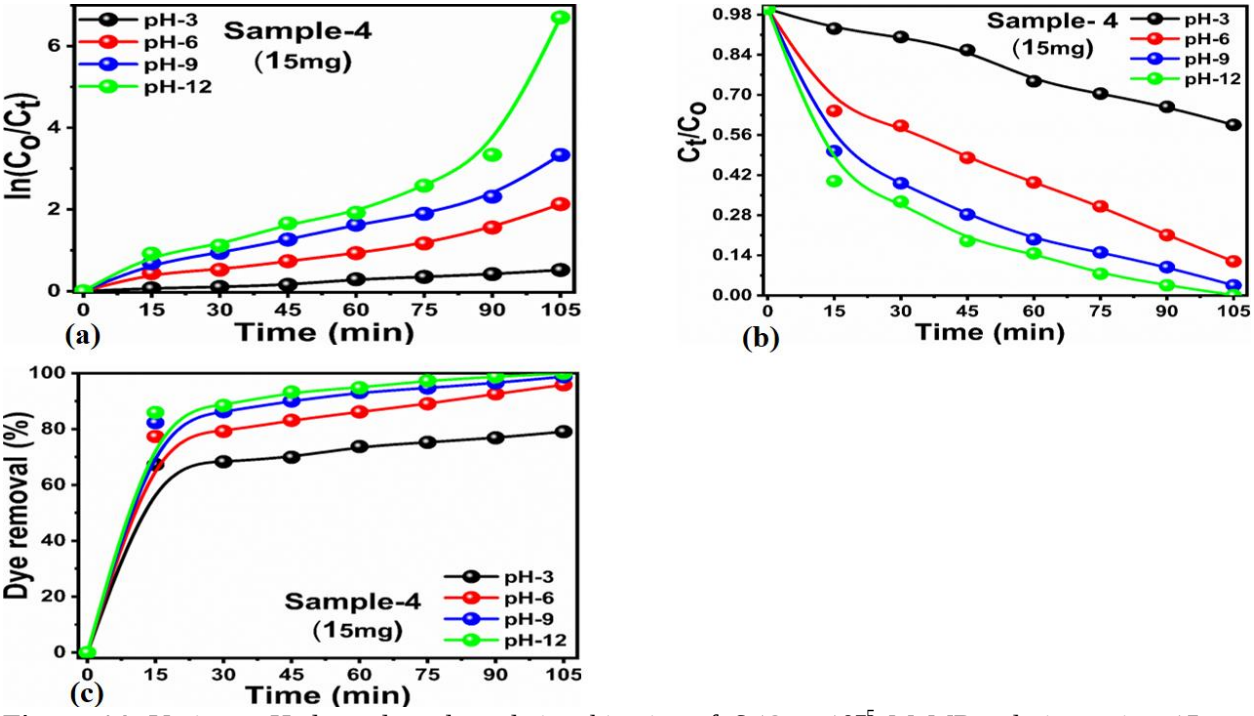

Figure 14. Various pH dependent degradation kinetics of 6.12×10^{-5} M MB solution using 15 mg catalyst dose of sample-4 under the irradiation of natural sunlight. (**a**) Linear plot of $Ln(C_t/C_o)$ against corresponding time of 105 min. (**b**) Linear plot of C_t/C_o. (**c**) Various pH dependent degradation efficiency of MB solution.

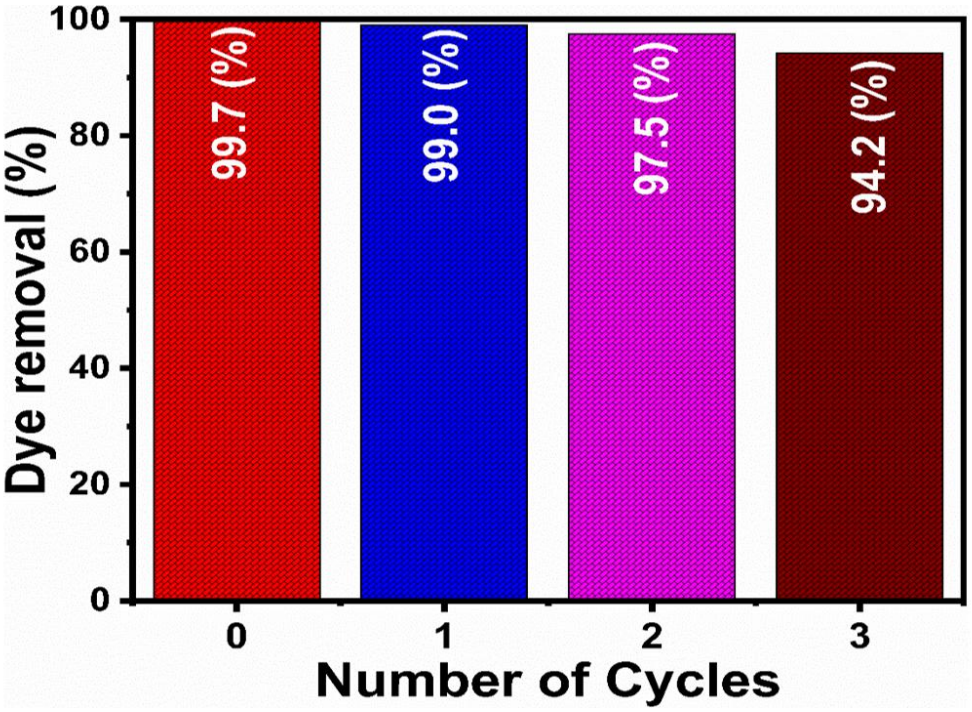

Figure 15. Reusability test of green synthesized ZnO (Sample-4) during the photodegradation of MB dye under the irradiation of natural sunlight irradiation

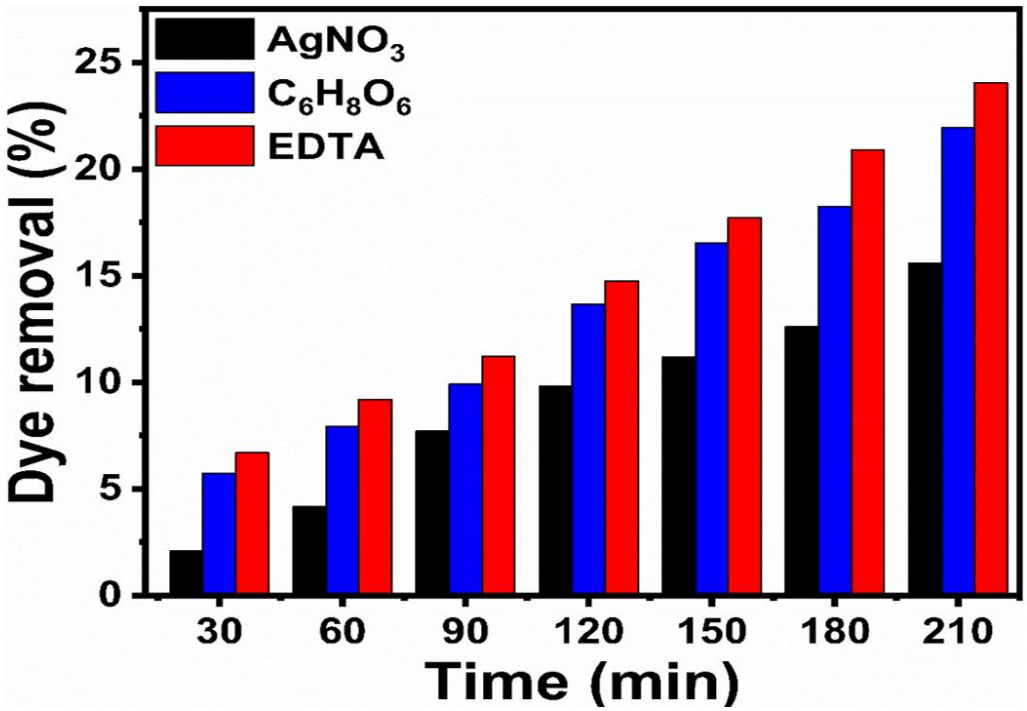

Figure 16. Dye removal efficiency of 8. 22×10^{-5} M MB solution in the presence of various scavengers

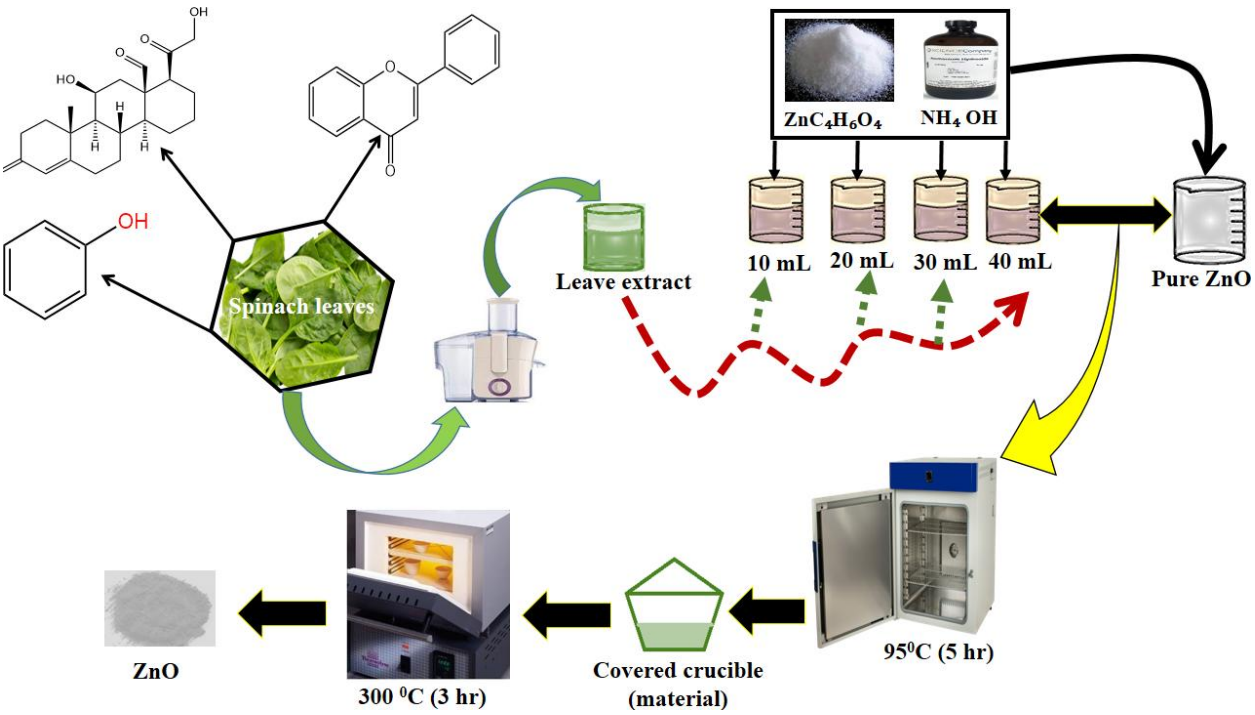

Scheme 1. Material synthesis illustration of as-synthesized ZnO samples treated with different amount of leafy extract of ***S. oleracea.***

Table 1. Samples with specifications

S.No	Sample. ID	Sample specification
1	Pure ZnO	0.1M, Zinc acetate dihydtae, 5mL ammonium hydroxide (25%)
2	Sample-1	0.1M, Zinc acetate dihydtae, 5mL ammonium hydroxide (25%) and 10 mL S. oleracea extract
3	Sample-2	0.1M, Zinc acetate dihydtae, 5mL ammonium hydroxide (25%) and 20 mL S. oleracea extract
4	Sample-3	0.1M, Zinc acetate dihydtae, 5mL ammonium hydroxide (25%) and 30mL S. oleracea extract
5	Sample-4	0.1M, Zinc acetate dihydtae, 5mL ammonium hydroxide (25%) and 40 mL S. oleracea extract

Table 2. Calculated average crystallite size (nm) for pure ZnO and green synthesized ZnO samples prepared in the presence of various amounts of leaf extract of *S. oleracea*

Name of Samples	2(θ)			Average particle size (nm)
	100	002	101	
Pure ZnO	31	33	34	19.6
10 ml	31.2	33.5	35.7	19
20 ml	31.5	33.8	35.9	18
30ml	31.8	34.2	36.4	16
40ml	32	35.8	36.9	14

Table 3. Summarized performance evaluation of pure ZnO and green synthesized ZnO samples against the dye removal of MB under the sun light irradiation.

Sample name	Catalyst Dose (mg)	Dye concentration	Dye removal (%)	Constant (K)
Sample-1	5mg	8.22×10^{-5} M	71.2	3.25×10^{-3} min^{-1}
Sample-2	5mg		83.5	5.95×10^{-3} min^{-1}
Sample-3	5mg		96.4	1.31×10^{-2} min^{-1}
Sample-4	5mg		97.2	1.42×10^{-2} min^{-1}
Sample-1	10mg	8.22×10^{-5} M	83.4	5.86×10^{-3} min^{-1}
Sample-2	10mg		92.3	8.72×10^{-3} min^{-1}
Sample-3	10mg		97.2	1.47×10^{-2} min^{-1}
Sample-4	10mg		98.4	1.77×10^{-2} min^{-1}
Pure ZnO	15mg		57.0	1.58×10^{-3} min^{-1}
Sample-1	15mg	8.22×10^{-5} M	91.8	9.68×10^{-3} min^{-1}
Sample-2	15mg		94.9	1.12×10^{-2} min^{-1}
Sample-3	15mg		98.7	1.18×10^{-2} min^{-1}
Sample-4	15mg		99.6	2.26×10^{-2} min^{-1}
Sample-4	5mg	6.12×10^{-5} M	95.8	1.18×10^{-2} min^{-1}
	10mg		97.0	1.33×10^{-2} min^{-1}
	15mg		99.7	2.54×10^{-2} min^{-1}
		pH Study		

Sample-4	15mg	pH-3	6.12×10^{-5} M	79.0	4.95×10^{-3} min^{-1}
	15mg	pH-6		95.8	1.79×10^{-2} min^{-1}
	15mg	pH-9		98.7	2.75×10^{-2} min^{-1}
	15mg	pH-12		99.9	5.05×10^{-2} min^{-1}

Table 4: Comparison of photocatalytic activity of synthesized ZnO NPs for MB with previous reported works.

Catalysts	**MB Dyes concentration (M)**	**Time(min)**	**Removal %**	**Reference**
ZnO NPs	5×10^{-5} M	180	74	[72]
ZnO -NPs	20 mg L^{-1}	120	81	[73]
(ZnO/NOC)	(10 mg/L)	150	98	[74]
(SBT-ZnO/NF)	15 mg/L	90	89	[75]
(St-ZnO)	20 mg/L	45	90	[76]
(CO–ZnO NPs)	(10 mg/L)	70	96	[77]
ZCP nano	(60mg/L)	20	84	[78]
(B–ZnO/TiO2)	(15 mg/L)	60	95	[79]

(CQD/N-ZnO)	(1.0×10^{-4} M)	90	90	[80]
Gd-dopedZnO:TiO2	(20 mg/L)	90	93	[81]
CuFe2O4@BC	5×10^{-5}	90	98.9	[82]
ZnO / spinach extract	(6.12×10^{-5} M)	105	99.6	Present work

References

[1]. Singh, J.; Dutta, T.; Kim, K.H.; Rawat, M.; Samddar, P.; Kumar, P. "Green" synthesis of metals and their oxide nanoparticles: applications for environmental remediation. J Nanobiotechnol. **2018,** 16, 1-24.

[2]. Singh, J.; Rathi, A.; Rawat, M.; Kumar, V.; Kim, K.H. The effect of manganese doping on structural, optical, and photocatalytic activity of zinc oxide nanoparticles. *Composites Part B: Engineering*, **2019,** *166*,361-370.

[3]. Moradnia, F.; Taghavi Fardood, S.; Ramazani, A.; Osali, S.; Abdolmaleki, I. Green sol–gel synthesis of CoMnCrO4 spinel nanoparticles and their photocatalytic application. *Micro & Nano Letters*. **2020,** *15*, 674-677.

[4]. Taghavi, F.; SaeidR, A.O.; Moradnia, F.; Afshari, Z.; Ganjkhanlu, S.; YekkeZare, F. Green synthesis of ZnO nanoparticles via Sol-gel method and investigation of its application in solvent-free synthesis of 12-Aryl-tetrahydrobenzo[α]xanthene-11-one derivatives under microwave irradiation. Chem Methodol. **2019,** 3,632–642.

[5]. Shah, A.P.; Jain, S.; Shimpi, N.G. Enhanced photocatalytic activity of electrospun PAN/Ag-G NFs under solar irradiation for effective degradation of hazardous organic dyes. ChemistrySelect. **2020,** 5, 3897–3905.

[6]. Jain, S.; Shah, A.P.; Shimpi, N.G. An efficient photocatalytic degradation of organic dyes under visible light using zinc stannate (Zn_2SnO_4) nanorods prepared by microwave irradiation. Nano-Struct Nano-Objects. **2020,** 21, 100410.

[7]. Khan, M.S.; Dhavan, P.P.; Jadhav, B.L.; Shimpi, N.G. Ultrasound-assisted green synthesis of Ag-Decorated ZnO nanoparticles using Excoecariaagallocha leaf extract and evaluation of their photocatalytic and biological activity. Chemistry Select. **2020,** 5, 2365–6549

[8]. Singh, J.; Kumar S.; Alok, A.; Upadhyay, S.K.; Rawat, M. D.C.W.; Tsang, B.N.; Ki-Hyun, K. The potential of green synthesized zinc oxide nanoparticles as nutrient source for plant growth. JClean Prod. **2019,** 214, 1061–1070.

[9]. Taghavi, F.S.; Moradnia, F.; Mostafaei, M.; Afshari, Z.; Faramarzi, V.; Ganjkhanlu, S. Biosynthesis of $MgFe_2O_4$ magnetic nanoparticles and its application in photodegradation of malachite green dye and kinetic study. Nanochem Res. **2019,** 4, 86–93.

[10]. Atrak, K.; Ramazani, A.; Taghavi, F. Green synthesis of $Zn_{0.5}Ni_{0.5}AlFeO_4$ magnetic nanoparticles and investigation of their photocatalytic activity for degradation of reactive blue 21 dye. Environ Technol. **2020,** 41, 2760–2770.

[11]. Wang. J.; Qiao, M.; Wei, K.; Ding, J.; Liu, Z.; Zhang, K.Q.; Huang, X. Decolorizing activity of Malachite Green and its mechanisms involved in dye biodegradation by *Achromobacterxylos oxidans* MG1. J Mol Microbiol Biotechnol. **2011,** 20, 220–227

[12]. Ravelli, D.; Dondi, D.; Fagnoni, M.; Albini A. Photocatalysis. A multi-faceted concept for green chemistry. ChemSoc Rev. **2009,** 38, 1999.

[13]. Yuvaraja, S.; Kumar, V.; Dhasmana, H.; Kumar, A.; Verma, A.; Jain, V.K. Ultraviolet detection properties of electrodeposited n-SnO_2 modified p-Si nanowires hetero-junction photodiode.J Mater Sci Mater Electron. **2019,** *30*, 7618-7628.

[14]. Taghavi, F.S.; Ramazani, A.; Woo Joo, S. Sol-gel synthesis and characterization of zinc oxide nanoparticles using Black Tea extract. JApplChem Res. **2017,** 11, 8–17.

[15]. Singh, J.; Kaur, S.; Kaur, G.; Basu, S.; Rawat, M. Biogenic ZnO nanoparticles: a study of blueshift of optical band gap and photocatalytic degradation of reactive yellow 186 dye under direct sunlight. Green Process Synth. **2018,** *8*,272-280.

[16]. Mishra, M.; Chun, D.M. α-Fe_2O_3 as a photocatalytic material: a review. ApplCatal A Gen. **2015,** 498,126–141.

[17]. Kaur, G.; Kaur, H.; Kumar, S.; Verma, V.; Jhinjer, H.S.; Singh, J.; Al-Rashed, S. Blooming approach: one-pot biogenic synthesis of TiO_2 nanoparticles using piper betle for the degradation of Industrial Reactive Yellow 86 dye. J InrgOrganometPolym Mater. **2020,** *31*, 1111-1119.

[18]. Singh, J.; Kaur, H.; Rawat, M. A novel green approach for the synthesis of tungsten oxide nanorods and its efficient potential towards photocatalytic degradation of reactive green 19 dye. J Mater Sci Mater Electron. **2018,** 29,13715–13722.

[19]. Ullah, H.; Mushtaq, L.; Ullah, Z.; Fazal, A.; Khan, A.M. Effect of vegetable waste extract on microstructure, morphology, and photocatalytic efficiency of ZnO–CuO nanocomposites. Inorg Nano-Met Chem. **2020,** 1–13.

[20]. Jha, M.; Ansari, S.; Shimpi, N.G. Ultrasonic assisted green synthesis of Ag:CdO nanocubes and nanospheres using Citrus limon leaves for efficient degradation of organic dyes. J IndEngChem. **2019,** 69, 269–284.

[21]. Su, T.; Shao, Q.; Qin, Z.; Guo, Z.; Wu, Z. Role of interfaces in two-dimensional photocatalyst for water splitting. ACS Catal. **2018,** 8, 2253–2276.

[22]. Alshorifi, F.T.; Alswat, A.A.; Mannaa, M.A.; Alotaibi, M.T.; El-Bahy, S.M.; Salama, R.S. Facile and green synthesis of silver quantum dots immobilized onto a polymeric CTS–PEO blend for the photocatalytic degradation of p-Nitrophenol. *ACS omega*. **2021,** *6*, 30432-30441.

[23]. Alshorifi, F.T.; Alswat, A.A.; Salama, R.S. Gold-selenide quantum dots supported onto cesium ferrite nanocomposites for the efficient degradation of rhodamine B. *Heliyon*, **2022,** *8*, e09652.

[24]. Alshorifi, F.T.; Ali, S.L.; Salama, R.S. Promotional synergistic effect of Cs–Au NPs on the performance of Cs–Au/MgFe2O4 catalysts in catalysis 3, 4-Dihydropyrimidin-2 (1H)-Ones and degradation of RhB Dye. *Journal of Inorganic and Organometallic Polymers and Materials*, **2022,** *32*, 3765-3776.

[25]. Sun, L.; Wang, Y.; He, L.; Guo, J.; Deng, Q.; Zhao, X.; Yan, Y.; Qi, K. Effect of cobalt doping on the photocatalytic performance of AgInS2 for organic pollutant degradation and hydrogen production. *Journal of Alloys and Compounds*. **2022,** *926*, 166859.

[26]. Gu, X.; Tan, C.; He, L.; Guo, J.; Zhao, X.; Qi, K.; Yan, Y. Mn2+ doped AgInS2 photocatalyst for formaldehyde degradation and hydrogen production from water splitting by carbon tube enhancement. *Chemosphere*. **2022,** *304*, 135292.

[27]. Song, J.; Zhang, J.; Zada, A.; Ma, Y.; Qi, K. CoFe2O4/NiFe2O4 S-scheme composite for photocatalytic decomposition of antibiotic contaminants. *Ceramics International*. **2022.**

[28]. Cui, Q.; Gu, X.; Zhao, Y.; Qi, K.; and Yan, Y. S-scheme CuInS2/ZnS heterojunctions for the visible light-driven photocatalytic degradation of tetracycline antibiotic drugs. *Journal of the Taiwan Institute of Chemical Engineers*. **2023,** 104679.

[29]. Zhang, J.; Gu, X.; Zhao, Y.; Zhang, K.; Yan, Y.; Qi, K. Photocatalytic Hydrogen Production and Tetracycline Degradation Using ZnIn2S4 Quantum Dots Modified g-C3N4 Composites. *Nanomaterials*. **2023,** *13*, 305.

[30]. Qi, K.; Zhuang, C.; Zhang, M.; Gholami, P.; Khataee, A. Sonochemical synthesis of photocatalysts and their applications. *Journal of Materials Science & Technology*. **2022,** *123*, 243-256.

[31]. Zhang, J.; Zhao, Y.; Zhang, K.; Zada, A.; Qi, K. Sonocatalytic degradation of tetracycline hydrochloride with CoFe2O4/g-C3N4 composite. *Ultrasonics Sonochemistry*. **2023,** 06325.

[32]. Khalid, N.; Majid, A.; Niaz, T.M.B.; Khalid, N.S. Carbonaceous-TiO_2 nanomaterials for photocatalytic degradation of pollutants: a review. Ceram Int. **2017,** 43, 14552–14571.

[33]. Singh, M.; Singh, J.; Rawat, M.; Sharma, J.; Singh, P.P. Enhanced photocatalytic degradation of hazardous industrial pollutants with inorganic–organic TiO_2–SnO_2–GO hybrid nanocomposites. J Mater Sci Mater Electro. **2019,** *30*, 13389-13400.

[34]. Singh, K.; Singh, J.; Rawat, M. Green synthesis of zinc oxide nanoparticles using Punica Granatum leaf extract and its application towards photocatalytic degradation of Coomassie brilliant blue R-250 dye. SN Appl Sci. **2019,** 1, 1-8.

[35]. Singh, J.; Kumar, S.; Alok, A.; Upadhyay, S.K.; Rawat, M.; Tsang, D.C.; Bolan, N.; Kim, K.H. The potential of green synthesized zinc oxide nanoparticles as nutrient source for plant growth. *Journal of Cleaner Production*, **2019,** *214*, 1061-1070.

[36]. Prami, N.; Debajyoti, D. Photocatalytic degradation of Rhodamine-B dye by stable ZnO nanostructures with different calcination temperature induced defects. Appl Surf Sci. **2019,** 465,546–556.

[37]. Alharthi, F.A.; Alghamdi, A.A.; Alothman, A.A.; Almarhoon, Z.M.; Alsulaiman, M.F.; Al-Zaqri, N. Green synthesis of ZnO nanostructures using salvadorapersica leaf extract: applications for photocatalytic degradation of methylene blue dye. Crystals. **2020,** 10, 441.

[38]. Jha, M.; Shimpi, N.G. Spherical nanosilver: bio-inspired green synthesis, characterizations, and catalytic applications. Nano-Struct Nano-Objects. **2018,** 16, 234–249.

[39]. Vinay, S.P.; Chandrasekhar, N. Structural and Biological Investigation of Green Synthesized Silver and Zinc Oxide Nanoparticles. J InorgOrganomet Polym Mater, **2020,** 1–7.

[40]. Singh, J.; Kumar, V.; Kim, K.H.; Rawat, M. Biogenic synthesis of copper oxide nanoparticles using plant extract and its prodigious potential for photocatalytic degradation of dyes. Environ Res. **2019,** 108569.

[41]. Lalitha, K.; Jong, C.; Ahn, E.; Jahan, R.; Suleman, A.; Jing, L.; Yang, D.C. Synthesis of panos extract mediated ZnO nano-flowers as photocatalyst for industrial dye degradation by UV illumination. J Photochem Photobiol. **2019,** 199,111588.

[42]. Ambasta, S.P. The useful plants of India. Publication and Information Directorate, Council of Scientific and Industrial Research, India, New Delhi. **1986,** 433–437.

[43]. Renganathan, S.; Samar, F.; Kalainila, P. Green synthesis of copper nanoparticles from para foetida leaf extract and its antibacterial activity. Asian J Pharm Clin Res. **2017,** 10, 79.

[44]. Suganya, D.; Rajan, M.R.; Ramesh, R. Green synthesis of iron oxide nanoparticles from leaf extract of passiflorafoetida and its antibacterial activity. Int J Curr Res. **2016,** 8, 42081–42085.

[45]. Mittal, A.K.; Chisti, Y.; Banerjee, U.C. Synthesis of metallic nanoparticles using plant extracts. Biotechnol Adv. **2013,** 31, 346–356.

[46]. Hanif, R.; Iqbal, Z.;Iqbal, M.; Hanif, S.; Rasheed, M. Use of vegetables as nutritional food: role in human health. *Journal of Agricultural and Biological Science*, **2006,** *1*, 18-22.

[47]. Lakshmi, S.J.; Bai, R.R.; Sharanagouda, H.; Ramachandra, C.T.; Nadagouda, S.; Doddagoudar, S.R. Biosynthesis and characterization of ZnO nanoparticles from spinach (Spinacia oleracea) leaves and its effect on seed quality parameters of greengram (Vigna radiata). *Int J Curr Microbiol App Sci*. **2017,** *6*, 3376-3384.

[48]. Djouadi, A.; Derouiche, S. Spinach mediated synthesis of zinc oxide nanoparticles: Characterization, In vitro biological activities study and in vivo acute toxicity evaluation. *Current Research in Green and Sustainable Chemistry*. **2021,** *4*, 100214.

[49]. Kisan, B.; Shruthi, H.; Sharanagouda, H.; Revanappa, S.B.; Pramod, N.K. Effect of nano-zinc oxide on the leaf physical and nutritional quality of spinach. *Agrotechnology*. **2015,** *5*, 135.

[50]. Moradnia, F.; Fardood, S.T.; Ramazani, A.; Gupta, V.K. Green synthesis of recyclable MgFeCrO4 spinel nanoparticles for rapid photodegradation of direct black 122 dye. *Journal of Photochemistry and Photobiology A: Chemistry*. **2020,** *392*, 112433.

[51]. Ahankar, H.; Taghavi Fardood, S.; Ramazani, A. One-pot three-component synthesis of tetrahydrobenzo [b] pyrans in the presence of Ni0. 5Cu0. 5Fe2O4 magnetic nanoparticles under microwave irradiation in solvent-free conditions. *Iranian Journal of Catalysis*. **2020,** *10*, 195-201.

[52]. Dizavandi, Z.R.; Aliakbar, A.; Sheykhan, M. Electrocatalytic determination of clopidogrel using Bi_2O_3-Pp-AP/GCE by differential pulse voltammetry in pharmaceutical productions. J Electroanal Chem. **2017,** 805, 24–31.

[53]. Rao, N.S.; Rao, M.V.B. Structural and optical investigation of ZnO nanopowders synthesized from Zinc Chloride and Zinc Nitrate. Am J Mater Sci. **2015,** 5, 66–68.

[54]. Bhatti, M.A.; Tahira, A.; Chandio, A.D.; Almani, K.F.; Bhatti, A.L.; Waryani, B.; Nafady, A.; Ibupoto, Z.H. Enzymes and phytochemicals from neem extract robustly tuned the photocatalytic activity of ZnO for the degradation of malachite green (MG) in aqueous media. *Research on Chemical Intermediates*, **2021,** *47*, 1581-1599.

[55]. Karthik, K.V.; Raghu, A.V.; Reddy, K.R.; Ravishankar, R.; Sangeeta, M.; Shetti, N.P.; Reddy, C.V. Green synthesis of Cu-doped ZnO nanoparticles and its application for the photocatalytic degradation of hazardous organic pollutants. *Chemosphere*, **2022,***287*, 132081.

[56]. Souri, M.; Hoseinpour, V.; Shakeri, A.; Ghaemi, N. Optimisation of Green Synthesis of MnO Nanoparticles via Utilising Response Surface Methodology. *IET Nanobiotechnol.* **2018,** *12*, 822–827.

[57]. Suwanchawalit, C.; Wongnawa, S. Influence of Calcination on the Microstructures and Photocatalytic Activity of Potassium Oxalate-Doped TiO_2 Powders. *Appl. Catal., A.* **2008,** *338*, (1-2), 87–99.

[58]. Suwanchawalit, C.; Wongnawa, S. Influence of Calcination on the Microstructures and Photocatalytic Activity of Potassium Oxalate-Doped TiO_2 Powders. *Appl. Catal., A.* **2008,** *338* (1-2), 87–99.

[59]. Li, F.-T.; Zhao, Y.; Liu, Y.; Hao, Y.-J.; Liu, R.-H.; Zhao, D.-S. Solution Combustion Synthesis and Visible Light-Induced Photocatalytic Activity of Mixed Amorphous and Crystalline $MgAl_2O_4$ Nanopowders. *Chem. Eng. J.* **2011,** *173*, 750–759.

[60]. Wang, F.; Min, S.; Han, Y.; Feng, L. Visible-light-induced Photocatalytic Degradation of Methylene Blue with Polyaniline-Sensitized TiO_2 Composite Photocatalysts. *Superlattices Microstruct.* **2010,** *48*, 170–180.

[61]. Kumar, N.; Mittal, H.; Reddy, L.; Nair, P.; Ngila, J.C.; Parashar, V. Morphogenesis of ZnO nanostructures: role of acetate (COOH−) and nitrate (NO 3−) ligand donors from zinc salt precursors in synthesis and morphology dependent photocatalytic properties. *RSC Advances*. **2015,** *5*, 38801-38809.

[62]. Marathe, Y.V.; Ramanna, M.M.V.; Shrivastava, V.S. Synthesis and characterization of nanocrystalline CdS thin films grown by chemical bath deposition at different molarities for removal of methylene blue. Desalin Water Treat. **2013,** 51, 5813–5820.

[63]. Shanthi, M.; Kuzhalosai, V. Photocatalytic degradation of an azo dye, Acid Red 27, in aqueous solution using nano ZnO. Ind J Chem. **2012,** 51, 428–434.

[64]. Mohammadzadeh, S.; Olya, M.E.; Arabi, A.M.; Shariati, A.; Khosravi, N.M.R. Synthesis, characterization and application of ZnO–Ag as a nanophotocatalyst for organic compounds degradation, mechanism and economic study. J Environ Sci. **2015,** 35,194–207.

[65]. Fatehah, M.O.; Aziz, H.A.; Stoll, S. Stability of ZnO nanoparticles in solution, influence of pH, dissolution, aggregation and disaggregation effects. J Coll Sci Biotechnol. **2014,** 3, 75–84.

[66]. Farrokhi, M.; Hosseini, S.; Yang, J.; Shirzad-Siboni, M. Application of ZnO–Fe_3O_4 nanocomposite on the removal of azo dye from aqueous solutions: kinetics and equilibrium studies. Water Air Soil Pollut. **2014,** 225, 1–12.

[67]. Akpan, U.G.; Hameed, B.H. Parameters affecting the photocatalytic degradation of dyes using TiO_2-based photocatalysts: a review. J Hazard Mater. **2009,** 170, 520–529.

[68]. Khairnar, S.D.; Patil, M.R.; Shrivastava, V.S. Hydrothermally synthesized nanocrystalline Nb_2O_5 and its visible-light photocatalytic activity for the degradation of congo red and methylene blue. Iran J Catal. **2018,** 8,143–150.

[69]. Jacob, J.M.; Rajan, R.; Aji, M.; Kurup, G.G.; Pugazhendhi, A. Bio-inspired ZnS quantum dots as efficient photo catalysts for the degradation of methylene blue in aqueous phase. Ceramics International. **2019,** 45, 4857-62.

[70]. Shelar, S.G.; Mahajan, V.K.; Patil, S.P.; Sonawane, G.H. Effect of doping parameters on photocatalytic degradation of methylene blue using Ag doped ZnO nanocatalyst. SN Applied Sciences. **2020,** 5**,** 1-0.

[71]. Mondol, B.; Sarker, A.; Shareque, A.M.; Dey, S.C.; Islam, M.T.; Das, A.K.; Shamsuddin, S.M.; Molla, M.; Islam, A.; Sarker, M. Preparation of activated carbon/TiO_2

nanohybrids for photodegradation of reactive red-35 dye using sunlight. Photochem. **2021,** 1, 54-66.

[72]. Osuntokun, J.; Onwudiwe, D.C.; Ebenso, E.E. Green synthesis of ZnO nanoparticles using aqueous Brassica oleracea L. var. italica and the photocatalytic activity. *Green chemistry letters and reviews*, **2019,** *12*, 444-457.

[73]. Bopape, D.A.; Motaung, D.E.; Hintsho-Mbita, N.C. Green synthesis of ZnO: Effect of plant concentration on the morphology, optical properties and photodegradation of dyes and antibiotics in wastewater. *Optik.* **2022,** *251*,168459.

[74]. Yu, S.; Zhou, J.; Ren, Y.; Yang, Z.; Zhong, M.; Feng, X.; Su, B.; Lei, Z. Excellent adsorptive-photocatalytic performance of zinc oxide and biomass derived N, O-contained biochar nanocomposites for dyes and antibiotic removal. *Chemical Engineering Journal*. **2023,** *451*, 138959.

[75]. Rupa, E.J.; Kaliraj, L.; Abid, S.; Yang, D.C.; Jung, S.K. Synthesis of a zinc oxide nanoflower photocatalyst from sea buckthorn fruit for degradation of industrial dyes in wastewater treatment. *Nanomaterials*. **2019,** *9*, 1692.

[76]. Bharathi, D.; Nandagopal, J.G.T.; Rajamani, R.; Pandit, S.; Kumar, D.; Pant, B.; Pandey, S.; Gupta, P.K. Enhanced photocatalytic activity of St-ZnO nanorods for methylene blue dye degradation. *Materials Letters*. **2022,** *311*, 131637.

[77]. Wu, Y.; Altuner, E.E.; Tiri, R.N.E.H.; Bekmezci, M.; Gulbagca, F.; Aygun, A.; Xia, C.; Van Le, Q.; Sen, F.; Karimi-Maleh, H. Hydrogen generation from methanolysis of sodium borohydride using waste coffee oil modified zinc oxide nanoparticles and their photocatalytic activities. *International Journal of Hydrogen Energy*. **2023,** *48*, 6613-6623.

[78]. Singh, A.R.; Dhumal, P.S.; Bhakare, M.A.; Lokhande, K.D.; Bondarde, M.P.; Some, S. In-situ synthesis of metal oxide and polymer decorated activated carbon-based photocatalyst for organic pollutants degradation. *Separation and Purification Technology*. **2022,** *286*, 120380.

[79]. Shathy, R.A.; Fahim, S.A.; Sarker, M.; Quddus, M.S.; Moniruzzaman, M.; Masum, S.M.; Molla, M.A.I. Natural sunlight driven photocatalytic removal of toxic textile dyes in water using B-doped ZnO/TiO2 nanocomposites. *Catalysts*. **2022,** *12*, 308.

[80]. Muthulingam, S.; Lee, I.H.; Uthirakumar, P. Highly efficient degradation of dyes by carbon quantum dots/N-doped zinc oxide (CQD/N-ZnO) photocatalyst and its compatibility

on three different commercial dyes under daylight. *Journal of colloid and interface science*. **2015,** *455*, 101-109.

[81]. Panwar, S.; Upadhyay, G.K.; Purohit, L.P. Gd-doped ZnO: TiO2 heterogenous nanocomposites for advance oxidation process. *Materials Research Bulletin.* **2022,** *145*, 111534.

[82]. Liu, X.; Shen, S.; Xu, C.; Li, X.; Zhu, L.; Wang, X. Studying photocatalytic dye degradation with bismuth nitrate–derived catalysts using paper microzones method. *Materials Today Chemistry*. **2022,** *23*, 100667.